Engineering Structures 307 (2024) 117853

Contents lists available at ScienceDirect

Engineering Structures

journal homepage: www.elsevier.com/locate/engstruct

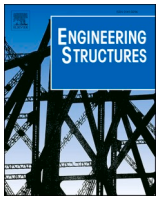

Issues related to typological fragility curves derivation starting from observed seismic damage

M. Tatangelo [a,*,1], L. Audisio [a,2], M. D'Amato [b,3], R. Gigliotti [a,4]

[a] DISG, Dept. of Structural and Geotechnics Engineering, Sapienza University of Rome, Via Eudossiana 18, 00184 Rome, Italy
[b] DiCEM, Dept. Of European and Mediterranean Cultures, Architecture, Environment and Cultural Heritage, University of Basilicata, Via Lanera, 75100 Matera, Italy

ARTICLE INFO

Keywords:
Database completion
Seismic damage
Fragility
Masonry buildings
Partitioning
Vulnerability

ABSTRACT

In this study typological fragility curves are proposed with a macro-seismic approach. To this scope, a stock of 56.338 residential masonry buildings struck by L'Aquila 2009 seismic sequence is analyzed, whose *AeDES* forms are archived within *Da.D.O.* platform, that is a web-gis database collecting the observed seismic damage data related to buildings surveyed after several Italian earthquakes.

Moreover, issues significantly influencing the fragility curves derivation are in depth discussed. In particular, a criterion for the buildings stock completion adding undamaged and not surveyed buildings is proposed, based on the distributions known of the residential building typologies. Comparisons highlight that the database completion affects the resulting fragility curves, and in particular for low damage levels. Furthermore, it is shown how the fundamental parameters estimation, by using the *Maximum Likelihood Estimation* (*MLE*) method, is conspicuously influenced by the *PGA* intervals number (n_{int}), that is an issue often ignored when fragility curves are derived. The numerical investigations show that, although a non-monotonic trend is observed, the fundamental parameters tend to converge to the asymptotic values as the n_{int} of *PGA* increases, and that they are markedly dispersed when n_{int} is low.

1. Introduction

In recent years many methods have been developed for designing and assessing seismic performance of a structure in a probabilistic manner. These methods, such as for instance the *Performance-Based Earthquake Engineering* (*PBEE*) further developed in *ATC-58* project [42,43], require the application of fragility curves in order to evaluate damage and losses due to seismic scenarios. Contrarily to the vulnerability curve providing a seismic loss (in terms of the direct damage cost, casualties, or downtime), a fragility curve measures a probability of exceeding a certain *Damage Level* (*DL*) or *Limit State* (*LS*) for a given *Intensity Measure* (*IM*) expressing the ground shaking [46]. Moreover, when a good quality of empirical loss data is not available, it is also possible to indirectly derive a vulnerability curve starting from a fragility curve by means of damage-to-loss functions [50].

Fragility curves have become undoubtedly an essential tool to compute and to prevent economic and social losses [13] within a probabilistic approach, where uncertainties of model (epistemic due to lack of knowledge) and aleatory (typically including record-to-record variability) may be taken into account [22].

To date, several approaches have been proposed in order to obtain structural fragility curves, essentially derived with two different approaches: numerical approaches, by using structural models to predict seismic damage [2,23,47,6,9]; macro-seismic approaches, based on damage survey (observational criterion) of a buildings stock after a certain seismic sequences (one or more) [11,14,24,39,59,60,68]. Recently, also a hybrid approach has been proposed by combining the information derived from observed damage with numerical analyses [36].

As regards numerical approaches, *Non-linear Dynamic Analysis* (*NDA*) with the *Incremental Dynamic Analysis* (*IDA*) procedure may be utilized [61]. To this scope, a set of accelerograms is chosen, amplified or scaled

* Corresponding author.
E-mail address: matteo.tatangelo@uniroma1.it (M. Tatangelo).
[1] ORCID: 0000-0001-5162-4073
[2] ORCID: 0000-0002-3232-0688
[3] ORCID: 0000-0003-3107-6262
[4] ORCID: 0000-0002-2967-192X

https://doi.org/10.1016/j.engstruct.2024.117853
Received 14 November 2023; Received in revised form 27 January 2024; Accepted 10 March 2024

to estimate the structural response for each shaking intensity. Similar results can be obtained with the *Multiple Stripe Analysis* (*MSA*) method, where accelerograms records are scaled in relation to a common *IM* [34], or with the *Cloud* method, where unscaled accelerations and linear regressions are used [12,35]. However, given complexity and high computational costs required, simplified tools for fragility curves construction have been proposed, too. Among these, in Baltzopoulos et al. [6] the *SPO2FRAG* approach has been presented, including the *SPO2IDA* presented [62] for deriving approximated *IDA* results from *Static Push-Over* (*SPO*) curves of *Non-linear Static Analyses* (*NSA*).

As for the macro-seismic approach, pioneer works were proposed since early 70's, in which the buildings seismic behaviour was expressed in probabilistic terms by means of *Damage Probability Matrices* (*DPMs*), derived from the observed damage. *DPMs* express in a discrete form the occurrence probability of certain *DL* conditioned to an *IM*. Among the others, in Whitman, Reed, & Hong [63] *DPMs* were defined for 9 damage categories due to San Fernando 1971 earthquake. Braga, Dolce, & Liberatore [8] defined *DPMs* according to the *Medvedev-Sponheuer-Karnik* (*MSK-76*) macro-seismic scale [44] of about 36.000 buildings surveyed after the Irpinia 1980 earthquake. In Sabetta, Goretti, & Lucantoni [55] the limitation due to the use of macro-seismic *IM* was eliminated, by applying the *MSK* scale with different parameters for deriving fragility curves starting from a stock of about 50.000 buildings struck by different Italian earthquakes. More recently, Zuccaro & Cacace [65] proposed *DPMs* by analysing about 170.000 buildings damaged by several Italian earthquakes, from Irpinia 1980 to Etna 2002. In order to permit the comparison among the different building stocks, in this study a new synthetic parameter was proposed, considering typological classes basically based on the vertical structure types.

Recently, rather than using *DPMs*, fragility curves are preferred because of they express a damage probability measure in a continuous form. To date, in literature a huge number of fragility curves are proposed starting from the seismic damage observed in past earthquakes, differing each other for several aspects such as: characteristics of buildings stocks considered, number and type of information, reference *IM* chosen. Among the others, one may mention the recent works of Rota, Penna, & Strobbia [54], Chieffo & Formisano [10], Del Gaudio et al. [16], Rosti, Rota, & Penna [53], Zuccaro et al. [66] and Biglari & Formisano [7].

As known, when macro-seismic approach is applied for deriving typological fragility curves buildings stock data completeness represents an important issue. This is due to the fact that, during the post-earthquake phase, seismic damage surveys are reasonably carried out on the totality of buildings only in the epicentral area. Conversely, far from the epicentre, post-earthquake surveys tend not to regard all buildings, but only the damaged ones. Therefore, an epistemic uncertainty (bias) is obtained on the observed data since information on undamaged buildings, since not surveyed, is unknown. Several Authors in literature have faced the building stock data completeness issue, proposing completion procedures in order to derive more reliable fragility curves. In Del Gaudio et al. [15] fragility curves are proposed considering only residential buildings located in municipalities with I_{MCS} higher than VI and surveyed according to Dolce & Goretti [18], by assuming that these municipalities were completely surveyed after L'Aquila 2009 earthquake. Procedures for including also municipalities affected by an earthquake, but not surveyed, are proposed in Del Gaudio et al. [16] and Rosti, Rota, & Penna [53]. In Zuccaro et al. [66], the database completion is performed considering a completeness index evaluated as a function of the *Peak Ground Acceleration* (*PGA*). Currently, in D'Amato et al. [14] and Laguardia et al. [39] a completion procedure is proposed based on the L'Aquila 2009 buildings stock and regarding municipalities having $I_{MCS} \leq$ VI. The procedure assumes that the completion of undamaged and not surveyed buildings follows the breakdown distribution of some reference municipalities, assumed completely surveyed.

To this it should be added that procedure adopted may significantly affect the fragility curves derived. As known, fundamental parameters estimation is done by maximizing the occurrence probabilities product of the observed seismic damages with *Maximum Likelihood Estimation* (*MLE*) method [5,40]. To date, although this method is largely applied in the scientific literature, influence of buildings stock damage partitioning for a given *IM* has not been duly argued yet, and how it may affect the fragility curves is frequently ignored. Concerning this topic, few indications may be found in literature. In Spence et al. [58] and Karababa & Pomonis [37] a minimum number of 20 buildings for each sub-sample of building damage is suggested. Whereas, Del Gaudio et al. [15] assumes that the sub-samples number is linked to the buildings stock size, so that the same buildings number is guaranteed in each sub-sample and for any *IM* range.

In this paper typological fragility curves with the macro-seismic approach are derived, by referring to the masonry buildings stock of L'Aquila 2009 earthquake available in *Da.D.O.* (*Observed Damage Database*) web-gis database ([21] *Dipartimento della Protezione Civile*; [20]). Starting from 74.049 buildings of 129 municipalities having *AeDES* forms [4] typological fragility curves are derived, by analysing only 56.338 buildings with a residential destination declared. Typological fragility curves are derived not only by referring to typological classes defined according to *AeDES* forms, but also considering the mixed ones having different horizontal structural elements. At first, a completion database procedure is proposed and applied, requiring additional information available in the Italian national census. This procedure provides a breakdown of undamaged and not surveyed masonry buildings belonging to all the structural typologies considered in the *AeDES* form. Moreover, attention is also paid to the choice of the sub-samples number when the buildings stock seismic damage is partitioned by varying a given *IM*. Finally, comparisons are illustrated and commented in order to highlight the importance of these issues in deriving the fragility curves with the macro-seismic approach.

2. Buildings stock of L'Aquila 2009 earthquake

On 6th April 2009, at 03:32 a.m. an earthquake of moment magnitude $M_w = 6{,}1$ [29] occurred, with the epicentre site near the city of L'Aquila (Italy) at a depth of 8,8 km in the Italian Abruzzi region [18]. The earthquake had in the epicentral area a macro-seismic intensity I_{MCS} = IX-X [57] according to *Mercalli-Cancani-Sieberg* (*MCS*) scale.

Survey activities were coordinated by the *Italian Civil Protection Department* (*D.P.C.*), starting from 7th April 2009. At first, strategic buildings were surveyed for immediate safe occupation in case of aftershocks [18]. Afterwards, surveys were extended also to residential buildings by using the rapid post-earthquake damage first level evaluation form, named *AeDES* form [4]. They were aimed at detecting seismic damage occurred, and at evaluating the usability of ordinary buildings after the earthquake. The *AeDES* forms compiled during L'Aquila 2009 surveys are nowadays available on *Da.D.O.* platform (*Observed Damage Database*, D.P.C., 2015; [20]), that is a web-gis database collecting the seismic damage data related to buildings surveyed during, or after, a seismic sequence having a national impact. Currently, *Da.D.O.* collects *AeDES* forms for the following earthquakes: Friuli 1976, Irpinia 1980, Abruzzo 1984, Umbria-Marche 1997, Pollino 1998, Molise 2002, Emilia 2003, L'Aquila 2009, Emilia 2012, Garfagnana-Lunigiana 2013, Centro Italia 2016–2017 and Mugello 2019.

AeDES form consists of several sections and, in particular, elaborations shown in this work are performed starting from data reported from *Section 1* to Section 4 of *AeDES* form.

In detail, Section 1 contains information concerning the building identification and its survey.

Section 2 collects data concerning age, construction period, metrical data, any building renovation, building use and its exposure (isolated or within an aggregate).

Section 3 is a fundamental section focused on some vulnerability indicators that may influence the seismic response of a building, mainly

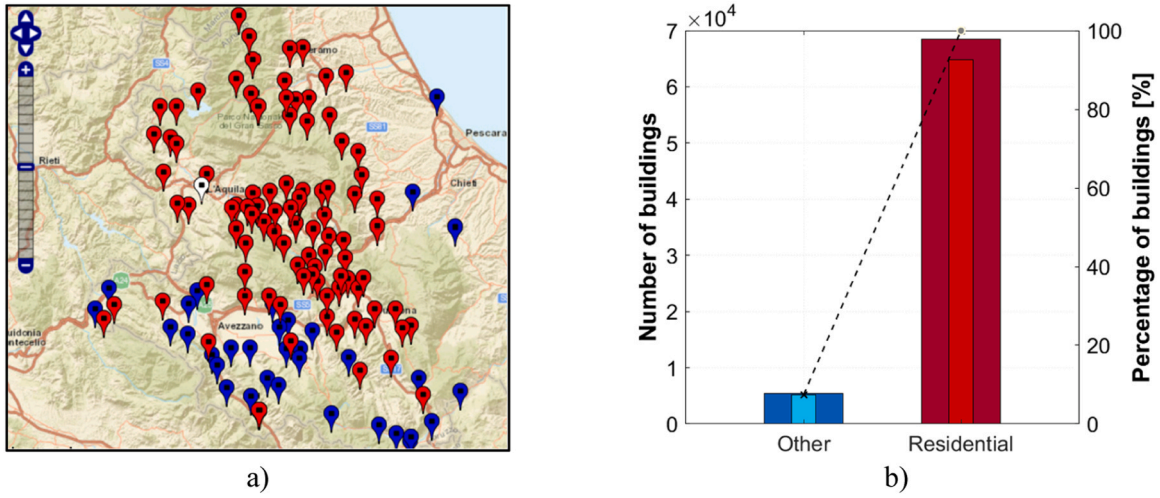

Fig. 1. (a) Municipalities where *AeDES* forms refer to residential buildings (red pins) and only to non-residential buildings (i.e. having public destinations, blue pins) respect to the mainshock epicenter (white pin); (b) Number and percentage of surveyed buildings: residential buildings (red histograms) and others (blue histograms).

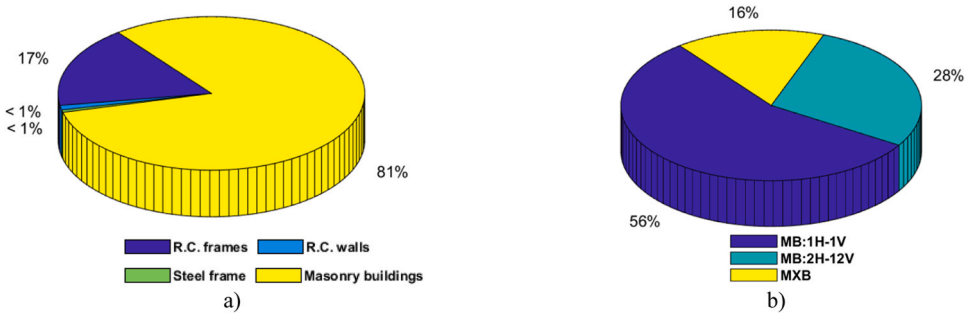

Fig. 2. (a) Percentage distribution for construction material of residential buildings surveyed after the L'Aquila 2009 earthquake; (b) Percentage distribution of residential masonry buildings surveyed by considering the type of vertical and horizontal structural element.

depending on the combination between vertical and horizontal structures. In this section a building may be classified in *Reinforced Concrete* (*RC*) or steel, only if the entire load-bearing structures are in one of these building materials. As for masonry buildings, it is possible to identify at the most two combinations of predominant horizontal and vertical structural components (the second should be reported only if present with a significant extent). Whereas, mixed masonry buildings are buildings having a combination of masonry and *RC*/steel elements. Section 3 considers five types of masonry for vertical structural elements: unidentified (*type A*); irregular texture and masonry of poor quality without (*types B*) and with (*type C)* tie-rods and tie-beams; or regular texture and masonry of good quality without (*types D*) and with (*type E)* tie-rods and tie-beams. This classification reflects the expected seismic behaviour, by assigning increasing seismic vulnerability to the masonry types for vertical structures considered. In particular, a regular texture tends to show a monolithic behaviour under seismic loads, excluding a local disaggregation of the masonry. While the presence of tie-rods and tie-beams contrast out-of-plane overturing failure mechanisms. According to the Section 3, the masonry vertical elements can be combined with six types of horizontal structural elements, that are: undefined members (*type 1*); vaults with/without tie-rods (*type 2*, *type 3*); and beams with flexible, semi-rigid and rigid slabs (*type 4*, *type 5,* and *type 6*). Even in the case of horizonal structural elements classification reflects different vulnerability levels of masonry buildings. As for vaulted floors, presence of tie-rods reduces as known the vertical loads thrust. As for slabs, they are differentiated with respect to their in-plane deformability and capacity to provide global box-like behaviour, in which out-of-plane overturning is prevented and seismic forces are distributed according to the in-plane stiffness of masonry walls. Horizontal structures having slabs from *type 4* to *type 6* tend progressively to provide a global box-like behaviour, with a reducing vulnerability passing from *type 4* to *type 6*. Finally, through the combination between vertical and horizontal structural elements previously defined it is possible to classify each building considered, identifying a specific structural typology to which correspond a certain level of seismic vulnerability. Therefore, typological classification provides useful information on the expected seismic vulnerability of a building.

Section 4 reports the damage detected with the visual inspection, that could be pre-existing or due to the seismic event. For each structural component (vertical structural elements, horizontal structural elements, stairs, roof and vertical partitions) a damage intensity is assigned according to the *EMS-98* scale [28], that are: D_0 (*null damage*), D_1 (*low damage*), D_2-D_3 (*moderate or heavy damage*), and D_4-D_5 (*very heavy damage or collapse*). Moreover, in this section damage level extent may be assigned, according to three percentage ranges of damage, such as *>2/3*, *1/3–2/3*, and *<1/3*, evaluated on the elements total number of the same type. For a more detailed description of the *AeDES* form sections the reader is referred to [4].

In total, as for the L'Aquila 2009 earthquake *Da.D.O.* collects *AeDES* forms of 74.049 buildings, located in 129 municipalities. More in detail, this stock consists of 68.556 buildings having an *AeDES* form with a declared residential destination. They fall in 95 of 129 municipalities suffered the earthquake swarm considered. While, the remaining 5.493 (74.049 – 68.556) buildings have a public destination, i.e. different from

Table 1
Masonry structures typologies (reported in *AeDES* form Section 3).

Vertical structural element / Horizontal structural element	Unidentified (A)	Irregular texture and poor quality		Regular texture and good quality	
		Without tie-rods and tie-beams (B)	With tie-rods and tie-beams (C)	Without tie-rods and tie-beams (D)	With tie-rods and tie-beams (E)
Unidentified (1)	1A	1B	1C	1D	1E
Vaults without tie-rods (2)	2A	2B	2C	2D	2E
Vaults with tie-rods (3)	3A	3B	3C	3D	3E
Beams with deformable slabs (4)	4A	4B	4C	4D	4E
Beams with semi-rigid slabs (5)	5A	5B	5C	5D	5E
Beams with rigid slabs (6)	6A	6B	6C	6D	6E

the residential one, located in 34 (129− 95) municipalities. Fig. 1a depicts the 95 municipalities where residential buildings were surveyed (red pins), and the remaining 34 (129− 95) ones where, instead, only other destinations were found (i.e., buildings having an *AeDES* form not reporting a residential destination, indicated with a blue pin). All inspections were coordinated by the *Italian Civil Protection Department*, that before building inspections defined 27 non-accessible zones, named "*red zones*" located in the L'Aquila historical centre and in the surrounding zones. Then, survey activities were initially extended to less damaged areas in order to limit the risks for surveyors in case of after-shocks, with the aim of identifying immediately usable buildings [27]. A higher priority was given to public buildings (schools, hospitals, industrial activities, etc.) than to residential ones, which were investigated only in municipalities with $I_{MCS} \geq$ VI and only upon request in other cases [18]. For completeness, Fig. 1b reports the corresponding buildings numbers (larger histograms), the related percentage (inner tighter histograms) and the cumulative percentage (dashed line).

The total number of residential buildings (68.556) represent about 93% of the buildings stock surveyed (74.049), whose breakdown percentage in terms of construction materials is indicated in Fig. 2a. It is easy to note that: the dominant typology is represented by masonry structures having 81% of occurrence percentage (56.338); the *RC* frame structures represent the 17% of the stock considered (11.715); whereas for steel frames and *RC* walls a percentage less than 1% is observed. An interesting result is obtained if one divides the sub-stock of masonry residential buildings (56.338) between buildings with only one type of vertical and horizontal structural element, and those having instead a mixed type of horizontal and/or vertical structural element, according to the typologies indicated in the Section 3 of the *AeDES* form (and reported in Table 1, where the number indicates the horizontal structural element and the letter the vertical one).

In this case it is found that (Fig. 2b):

- 56% of *Masonry* residential *Buildings* (*MBs*) has one type of horizontal and vertical structural element, briefly indicated in Fig. 2b as *MB:1H-1V*;
- 28% of *MBs* has a combination of two types of horizontal structural element and one or two types of vertical structural element, indicated as *MB:2H-12V*. It is considered that *MB:2H-12V* = *MB:2H-1V* + *MB:2H-2V* where *MB:2H-1V* and *MB:2H-2V* refer to buildings with one or two types of vertical structural element;
- 16% of buildings with mixed types of vertical structural element (e.g. masonry-*RC*, masonry-steel, reinforced masonry, etc.), and one or two horizontal structural elements (*MXB*).

56.338 residential buildings may be further analysed by considering the vertical structural element occurrence. To this scope, Fig. 3a shows the percentage distribution of masonry buildings with one vertical and horizontal structural element (buildings *MB:1H-1V* with 56% of Fig. 2b), where *type A* to *E* identify the vertical structural element according to Table 1. Fig. 3a indicates that the most frequent vertical structural element results the *type B* having a 46% (14.520 buildings) of occurrence; while the *types C* to *E* are present with percentages of 13%, 16% and 22%, respectively. Finally, one may note that 3% of vertical structures are unidentified (*type A*, 1.090 buildings). Whereas, Fig. 3b refers to the masonry buildings *MB:2H-12V* representing the 28% of Fig. 2b, having a combination of two horizontal structural elements and one (*types B* to *E*) or two vertical structural elements (*type A-2VS*). In this case, we obtain: 53% of *type B* (8.451), 23% of *type A-2VS*, 13% of *type C*, 7% of *type D* and 4% of *type E*. It is worth to note that the *type A-2VS* includes the residential buildings having *type A* or two types of masonry vertical structural elements, too.

Furthermore, residential buildings stock (Fig. 3) may be also analysed in accordance with the possible combinations among horizontal and vertical structural elements of the *AeDES* form (Table 1). Fig. 4 refers to residential masonry buildings with one type of horizontal and vertical structural element *MB:1H-1V* (Fig. 2b; Fig. 3a). It reports the horizontal structural element distribution (*type 1* to *6* of Table 1) for each type of vertical structural element (such as *types B* to *E* in Fig. 4a-d, respectively). In this analysis buildings with unidentified masonry (*type A*) are neglected. Each histogram of Fig. 4 reports the buildings numbers (wide bars) and the related percentage (narrow bars). Finally, in each histogram a dashed line is depicted as well, representing the cumulative percentage. It is clear to observe that in the buildings stock analysed

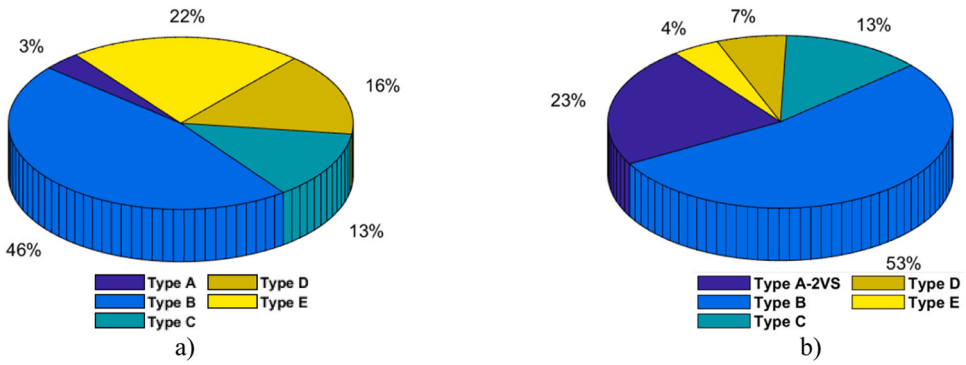

Fig. 3. Masonry buildings with (a) one type of horizontal and vertical structural element (*MB:1H-1V*); (b) two horizontal structural elements and one or two types of vertical structural element (*MB:2H-12V*).

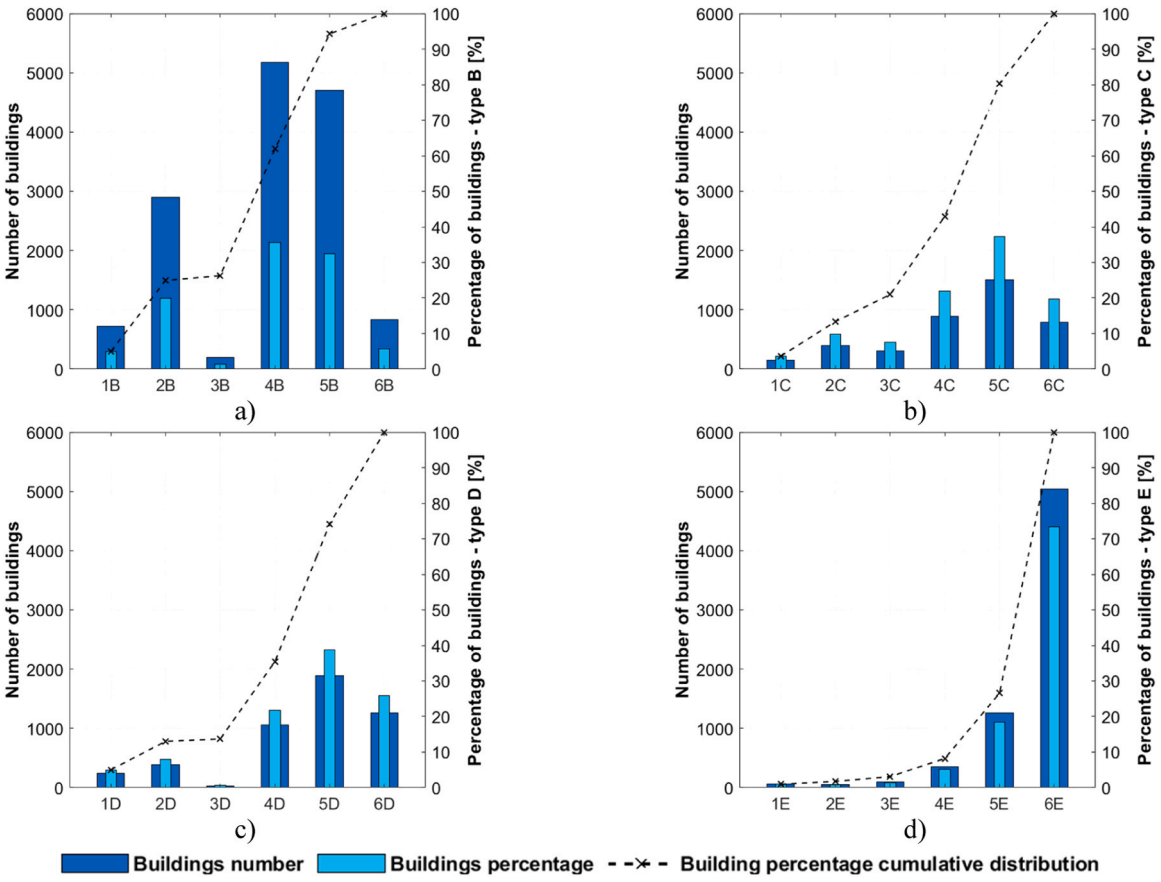

Fig. 4. *MB:1H-1V*. Residential buildings having a vertical structural element of: (a) *type B*; (b) *type C*; (c) *type D*; (d) *type E*, by varying the type of horizontal structural element (from *1* to *6* according to the Table 1).

masonry of poor quality (*type B* of Fig. 4a) is the dominant vertical structural element, combined with vaults (*type 2B*, 2.895 buildings, ≅ 20%), beams with deformable slabs (*type 4B,* 5.172 buildings, ≅35%), and beams with semi-rigid slabs (*type 5B*, 4.700 buildings, 30%).

Similarly, Fig. 5 shows the percentage distribution of masonry buildings with two types of horizontal and one type of vertical structural elements *MB:2H-1V*. It considers several combinations of two horizontal structural elements (*type 1* to *6* of Table 1) for each type of vertical structural element (such as *types B* to *E* in Fig. 5a-d, respectively). In this case the most frequent horizontal structural elements combinations are *types 2B–4B*, *2B–5B*, *4B–5B*, *2C-5C* with, respectively, 2.980, 2.871, 871 and 541 buildings.

As previously mentioned, the Section 4 of the *AeDES* form [4] classifies seismic damage to be assigned to each structural component in four levels, that are D_0, D_1, D_2-D_3 and D_4-D_5, based on *EMS-98* scale and *GNTD* survey forms [25,26]. A description of these seismic damage levels referred to masonry buildings is given in Table 2. Examples of seismic damages suffered by masonry buildings during L'Aquila 2009 earthquake may be found, among the others, in Augenti & Parisi, [3], Rossetto et al. [51] and Indirli et al. [30].

The damage levels considered are assigned to each structural component, such as: vertical structures, floors, stairs, roofs, partitions and considering pre-existing damage before the occurred seismic event. For instance, Fig. 6 reports a distribution analysis of the damage level among the structural components of residential masonry buildings stock considered (56.338), referring to *MB:1H-1V* (Fig. 6a and previously plotted in Fig. 4) and *MB:2H-1V* (Fig. 6b, previously plotted in Fig. 5). In both the typological classes analysed we obtain percentages quite similar for vertical structural element, that are in this case: damage level D_1 ≅ 25%, D_2-D_3 ≅ 20%, and D_4-D_5 ≅ 18%.

Once the damage level of each structural component is known a global building damage may be assigned. Firstly, it is necessary to convert the damage level of each structural component reported within *AeDES* form into *EMS-98* scale, where damage is classified into six different levels, that are: D_0 (*null damage*), D_1 (*negligible to slight damage*), D_2 (*moderate damage*), D_3 (*substantial to heavy damage*), D_4 (*very heavy damage*) and D_5 (*destruction*). Table 3 reports the conversion used, developed by the *Institute for Buildings Technology of the National Council of Research* (*CNR-ITC*) where, for a given structural component, a resulting *EMS-98* damage level is associated considering several combinations of damage and extension starting from the *AeDES* form damage level available [20].

Then, a global building damage may be estimated starting from the structural elements damage. To this scope several Authors proposed different criteria for the global damage estimation. In Di Pasquale & Goretti [17], Angeletti et al. [1] and Lagomarsino, Cattari, & Ottonelli [38] the building damage is calculated as the *Weighted Sum* (*WS* criterion) of the components damage, each of which having a specific weight. Instead, Rota, Penna, & Strobbia [54] assign the global damage by considering only the *Maximum Damage* (*MD* criterion) observed among the structure primary components, such as vertical and horizontal structural elements, and roofs. In this study the global damage is estimated according to the *MD* criterion because of, usually, usability assessment and reconstruction costs are mainly influenced by the most damaged structural element [54]. Furthermore, it is worth noting that with the *MD* criterion a more conservative approach is followed, since an overestimation of the global damage is obtained with respect to the *WS* criterion. Moreover, the *MD* criterion permits a faster seismic damage evaluation, since only few structural elements are analysed, that are vertical and horizontal structural elements, and roofs. Details about

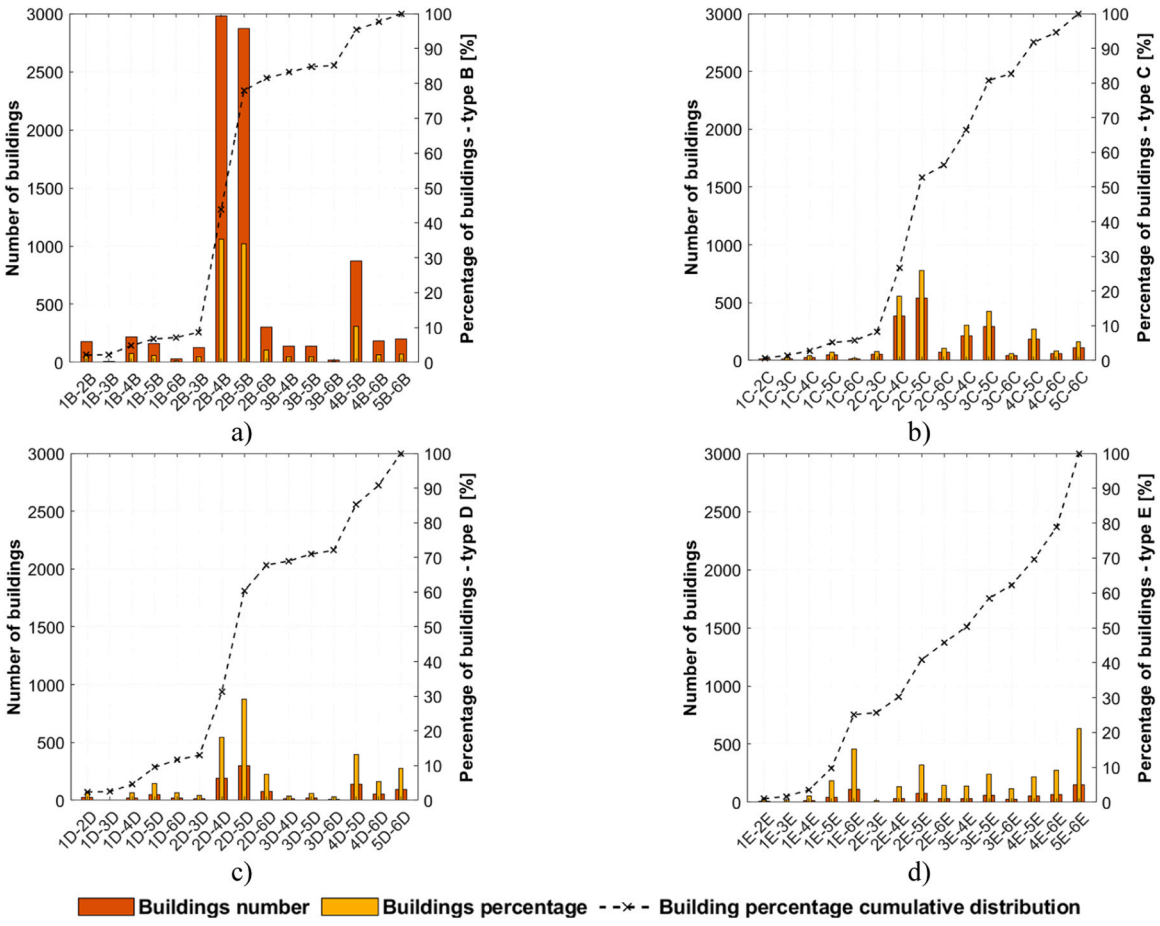

Fig. 5. *MB:2H-1V.* having a vertical structural element of: (a) *type B*; (b) *type C*; (c) *type D*; (d) *type E*, for several combinations of two horizontal structural elements (from types from *1* to *6* according to the Table 1).

Table 2
Damage level description for structural components of masonry buildings according to [4].

Damage Level	Damage description
D_0	*No damage.* This damage level may be assigned also in the case of plaster cracks due to shrinkage or small instability occurred in the past, repaired and not reactivated.
D_1	*This damage does not significantly affect structure capacity and it does not threaten the occupants safety.* It is associated to cracks having width ≤1 mm. No matter how they are distributed in masonry walls and in floors, without material expulsion, limited separations, or slight dislocations (≤1 mm) between parts of structures. Limited damage to the most flexible roofs with consequent falling of some tiles at the edges. Falling of small portions of degraded plaster or stucco, not connected to the masonry.
D_2-D_3	*With this damage the structure capacity significantly changes, without getting close to the limit of partial collapse of the main structural components with possible falling of non-structural objects.* Severe cracks, also with material expulsion, having a wide up to approximately 1 cm, symptoms of cracks due to crushing, significant separations between floors and/or stairs and walls and between orthogonal walls, some partial collapses in the secondary floors beams. Cracks of some mm in the vaults, and/or with symptoms of crushing. In roofs falling of a significant portion of the tiles covering.
D_4-D_5	*With this damage the structure capacity significantly changes, bringing it close to the limit of partial or total collapse of the main structural components.*

the *MD* criterion adopted in this study may be found in D'Amato et al., [14].

3. Ground motion intensity measure

The choice of an appropriate *IM* is very important for correlating the building seismic damage to *Ground Motion* (*GM*) intensity. In general, several *IMs* may be used such as: macro-seismic intensity measure, a discrete measure that may be affected by the surveyor judgment, expressed for instance with the *Modified Mercalli Intensity* (*MMI*) [64] or *European Macroseismic Scale* (*EMS*) [28]; or instrumental measures, such as the *PGA* or *Peak Ground Velocity* (*PGV*). The use of macro-seismic intensity as *IM* has been largely applied in the scientific literature since a good correlation with the observed damage has been observed. To this it should be added that data referred to this *IM* are widespread available before instrumental devices application. Nevertheless, several disadvantages may be encountered if one refers to the macro-seismic intensity measure. Firstly, if vulnerability and fragility curves consider different intensity scales a comparison among them cannot be directly performed. Moreover, macro-seismic intensity scale consider unit intervals that may not be equal, and fractional values are not considered. Finally, in literature few *Ground-Motion-to-Intensity-Conversion Equations* (*GMICEs*) are available [46], introducing additional uncertainties within the risk assessment framework [50]. These drawbacks may be solved by selecting an appropriate instrumental measure as *IM*. In this way, it is also possible to decouple the uncertainties related to the seismic demand from the ones introduced by the fragility curves. Among these, *PGA* is traditionally the main parameter chosen, even because commonly used for defining seismic loads for structures and hazard maps [54,55].

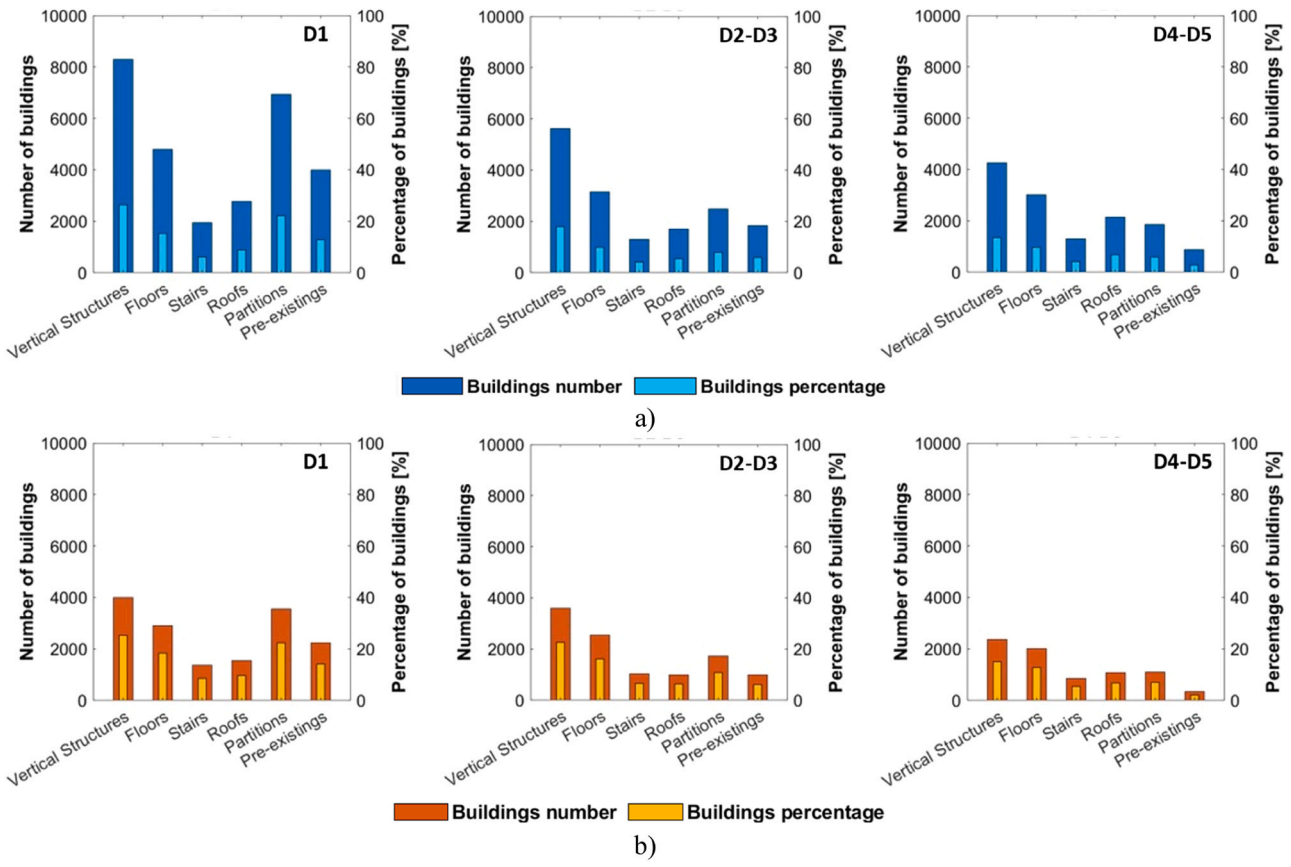

Fig. 6. Damage distributions of residential buildings components surveyed after L'Aquila 2009 earthquake: (a) *MB:1H-1V* buildings; (b) *MB:2H-1V*.

However, it may be not appropriate for correlations with the observed seismic damage, especially in the case of ductile structures or large damage states [49]. *PGV* should be more adequate in the case of deformable structures (when *PGA* becomes not adequate), but it is calculated with a direct integration of accelerograms and, therefore, it may be sensitive of record noise content and filtering process. Moreover, very few *PGV* attenuation functions are available in literature. The same limitations are to date encountered for the *Peak Ground Displacement* (*PGD*) [50].

Recently, there is a widespread use of Shaking map (also known as shake-map) providing an immediate visualization of the shaking level in a certain area affected by a seismic event. It is based on the interpolation algorithm of the registered *GMs* data and seismologic knowledge gathered from instrumental measures, taking into account local amplification effects through *S-wave* velocities in the upper 30 m (V_{S30}) [45]. A shake-map may display, for instance, *PGA*, *PGV*, *Spectral-Acceleration* of the 1^{th} vibration mode $Se(T_1)$ values, or a macro-seismic intensity estimated from the data measured. Moreover, as alternative to the shake-maps, attenuation laws may be used. Among the others, recently in literature D'Amato et al. [14] and Laguardia et al. [39] proposed attenuation laws derived from L'Aquila 2009 earthquake, considering as *IM* the *Arias Intensity* (I_A), or else the $Se(T_1)$, giving the opportunity of evaluating these *IMs* for several periods that are not available to date within the shake-maps.

In this study, *PGA* is used as *IM*, indicated in the shake-map proposed by INGV [31] for L'Aquila 2009 earthquake. However, it should be noted that this earthquake was characterized by a seismic sequence having several epicentral sites with a similar magnitude. Fig. 7a shows their location during the earthquake swarm, related to the shocks of 6^{th} April 2009 at 03:32 a.m. ($M_w = 6{,}1$), 6^{th} April 2009 at 11:15 p.m. ($M_w = 5{,}0$), 7^{th} April 2009 at 05:47 p.m. ($M_w = 5{,}4$), 9^{th} April 2009 at 12:52 a.m. ($M_w = 5{,}2$) and 9^{th} April 2009 at 07:38 p.m. ($M_w = 5{,}0$). While Fig. 7b-d reports the *PGA* shake-maps related to the mainshock on 6^{th} April 2009 ($M_w = 6{,}1$), and the aftershocks on 7^{th} April 2009 ($M_w = 5{,}4$) and 9^{th} April 2009 ($M_w = 5{,}0$) [31], respectively. In the same figures masonry buildings surveyed are located with black dots, too.

As one may clearly note, in the case of L'Aquila 2009 seismic sequence, the *i-th* building may have undergone in the aftershocks a *PGA* greater than the one suffered at the mainshock (6^{th} April 2009, $M_w = 6{,}1$). As proof of this, Fig. 8a depicts, by varying distance from the mainshock epicenter, the *PGA* maximum value (PGA_{max}) suffered by the 56.338 residential masonry buildings considered. In this figure black dots are used when the maximum value corresponds to the value occurred at the MainShock (6^{th} April 2009, $M_w = 6{,}1$), i.e. PGA_{max}=PGA_{MS}. While, red dots are used when the maximum value occurred during the AfterShocks from 6^{th} April 2009 ($M_w = 5{,}0$) to 9^{th} April *2009* ($M_w = 5{,}0$), i.e. PGA_{max}=PGA_{AS}. As one may clearly note, for many buildings the *PGA* suffered during the aftershocks was greater than the mainshock one.

In this study, the *PGA* suffered by each building is considered as the maximum value experienced during the entire seismic sequence. This assumption is mainly due to the fact that: all shocks of the seismic sequence occurred only in three days distant (6^{th}-9^{th} April 2009); almost the totality of the buildings stock was surveyed after the 9^{th} April because of the seismic sequence was really short (the inspection date is known on *AeDES* form). Similar approaches may be found in Rossi et al. [52], Ioannou et al. [32] and Zucconi, Romano, & Ferracuti [68]. In order to quantify the importance of this issue in the case of L'Aquila 2009 earthquake, Fig. 8b reports the percentage distribution related to 56.338 masonry residential buildings surveyed, indicating the buildings suffering a $PGA_{max} = PGA_{MS}$ (94%, 52.958 buildings), and the ones suffering a $PGA_{max} = PGA_{AS}$ (6%, 3.382 buildings). These buildings are also reported in the map of Fig. 8c, where it easy to note that the

Table 3
Conversion into *EMS-98* damage levels for *AeDES* form damage levels.

Damage level	Damage description	Damage levels conversion
D0	**Null damage** *no structural damage and no non-structural damage*	**D0**
D1	**Negligible to slight damage** *no structural damage and slight non-structural damage*	**D1** (<1/3) **D1** (1/3-2/3) **D1** (>2/3)
D2	**Moderate damage** *slight structural damage and moderate non-structural damage*	**D2** (<1/3) **D1** (<1/3) - **D2** (<1/3) **D1** (1/3-2/3) - **D2** (<1/3) **D1** (>2/3) - **D2** (<1/3)
D3	**Substantial to heavy damage** *moderate structural damage and heavy non-structural damage*	**D1** (<1/3) - **D2** (1/3-2/3) **D1** (1/3-2/3) - **D2** (1/3-2/3) **D2** (1/3-2/3) **D2** (>2/3) **D1** (<1/3) - **D2** (>2/3) **D3** (<1/3) **D1** (<1/3) - **D3** (<1/3) **D1** (1/3-2/3) - **D3** (<1/3) **D1** (>2/3) - **D3** (<1/3) **D2** (<1/3) - **D3** (<1/3) **D1** (<1/3) - **D2** (<1/3) - **D3** (<1/3)
D4	**Very heavy damage** *heavy structural damage and very heavy non-structural damage*	**D2** (1/3-2/3) - **D3** (<1/3) **D2** (>2/3) - **D3** (<1/3) **D3** (1/3-2/3) **D1** (<1/3) - **D3** (1/3-2/3) **D1** (1/3-2/3) - **D3** (1/3-2/3) **D2** (<1/3) - **D3** (1/3-2/3)
D5	**Destruction** *very heavy structural damage*	**D2** (1/3-2/3) - **D3** (1/3-2/3) **D3** (>2/3) **D1** (<1/3) - **D3** (>2/3) **D2** (<1/3) - **D3** (>2/3)

buildings with a $PGA_{\max} = PGA_{AS}$ are located near the aftershocks epicenters, and withitn a distance interval between 20 and 30 km from the mainshock epicenter. Moreover, for completeness Fig. 8d plots the difference percentage $\Delta_{PGA} = (PGA_{\max} - PGA_{MS})/PGA_{MS}(\%)$, by varying the distance from the mainshock epicentre. It is easy to note that the 6% of masonry residential buildings (Fig. 8b) during the aftershocks has registered a *PGA* value up to 60% higher than the mainshock one (PGA_{MS}).

For these reasons, in this study we refer to the PGA_{max} values suffered by any residential masonry building during L'Aquila 2009 seismic sequence, obtained as the envelope among the *PGA* shake-maps proposed in INGV [31]. Moreover, currently no information in *AeDES* forms is available on the evolution of the building seismic damage during this seismic sequence.

4. Fragility curves

A fragility curve provides the conditional probability that a *Damage* (D) takes place for a given *IM* value, reaching or exceeding a certain value (D_i). One of the most widely adopted representation for the fragility curve is the log-normal cumulative distribution function (Eq. 1). This distribution is very commonly used for fragility curves because of it is asymmetric about the mean and skewed to the left, reflecting better the frequency distribution of a certain *IM*, such as the *PGA*. The fragility function has the following expression [50]:

$$P_{D\geq D_i} = P(D \geq D_i|IM) = \Phi\left[\frac{\ln\left(\frac{IM}{\vartheta}\right)}{\beta}\right] \quad i = 1, \ldots, 5 \tag{1}$$

where $P_{D\geq D_i}$ is the fragility curve for *i-th* damage D_i; Φ is the standard normal cumulative distribution, ϑ and β are, respectively, *IM* median value and *IM* logarithmic values standard deviation.

The fundamental parameters (ϑ, β) are estimated through the *Maximum Likelihood Estimation* (*MLE*) method, allowing us of maximizing the observed damage data occurrence probability [40,5,56]. According to this method it is possible, within a certain buildings stock and for each typological class, to partition the sample available in several intervals (i.e. sub-samples) having a constant amplitude $\Delta IM = IM_{\max}/n_{\text{int}}$, where $IM_{\max}$ is the maximum *IM* available, and n_{int} the intervals number chosen. The *j-th* interval (bin) is given by $IM_j \pm \Delta IM/2$, centred on the mean value IM_j, including buildings stock damage from D_0 to D_5 [5]. In this study uncertainties due to the estimation on the shake-map of the *IM* considered were not taken into account.

Then, the likelihood function $\mathscr{L}_j$ in the *j-th* sub-sample is defined with the binomial probability distribution function (Eq. 2) to be maximized to find the fragility curve fundamental parameters:

$$\mathscr{L}_j = \binom{k_j}{z_j} \bullet p_j^{k_j} \bullet (1-p_j)^{z_j - k_j} \tag{2}$$

where k_j is the buildings number having a damage greater or equal than a specific damage level ($D_0, D_1, \ldots, D_5$); z_j is the buildings number in the *j-th* sub-sample; p_j is the probability of exceedance of the damage D_i expressed with the Eq. 1.

Finally, by considering the independence among the sub-samples data, the parameters ϑ_i and β are obtained by maximizing the product of the likelihood functions (Eq. 2), expressed logarithmic form [46] as follows:

$$(\vartheta_1, \ldots, \vartheta_5, \beta) = arg\max \sum_{i=1}^{5}\sum_{j=1}^{m} \left\{ \ln\binom{k_j}{z_j} + k_j \bullet \ln\left[\Phi\left(\frac{\ln\left(\frac{IM}{\vartheta_i}\right)}{\beta}\right)\right] + (z_j - k_j) \bullet \ln\left[\Phi\left(\frac{\ln\left(\frac{IM}{\vartheta_i}\right)}{\beta}\right)\right] \right\} \tag{3}$$

where $(\vartheta_1, \ldots, \vartheta_5, \beta)$ indicate, respectively, the median value and the logarithmic standard deviation of *IM* values for each D_i. In order to prevent the fragility curves intersection, a unique *IM* logarithm values standard deviation (β) is considered for all the curves [46].

5. Undamaged buildings estimation

The statistical elaborations presented in Sect. 2 refer to the masonry residential buildings stock available in the *Da.D.O.* database for L'Aquila 2009 earthquake that is, as already discussed, composed by buildings surveyed after the mainshock of 6th April 2009.

However, it is reasonable to expect that the buildings stock considered results incomplete, in the sense that it does not represent all the buildings that suffered the L'Aquila 2009 earthquake, but only the ones inspected to which an *AeDES* form was assigned. In other words, it could exist a certain number of not surveyed and, very likely, undamaged buildings after L'Aquila 2009 seismic sequence not included within the buildings stock considered in this study. Therefore, if one would perform a more reliable analysis of the seismic damage observed, also undamaged buildings should be taken into account requiring, hence, a database completion.

In this study, as discussed in the previous sections, the buildings stock for deriving fragility curves consists of 56.338 masonry residential buildings, falling into 95 municipalities having an *AeDES* form. This buildings stock is compared with the information collected in the *15th* database census conducted by the *Italian National Statistics Institute* [33] in 2011, since it is the closest database to the 2009 when L'Aquila

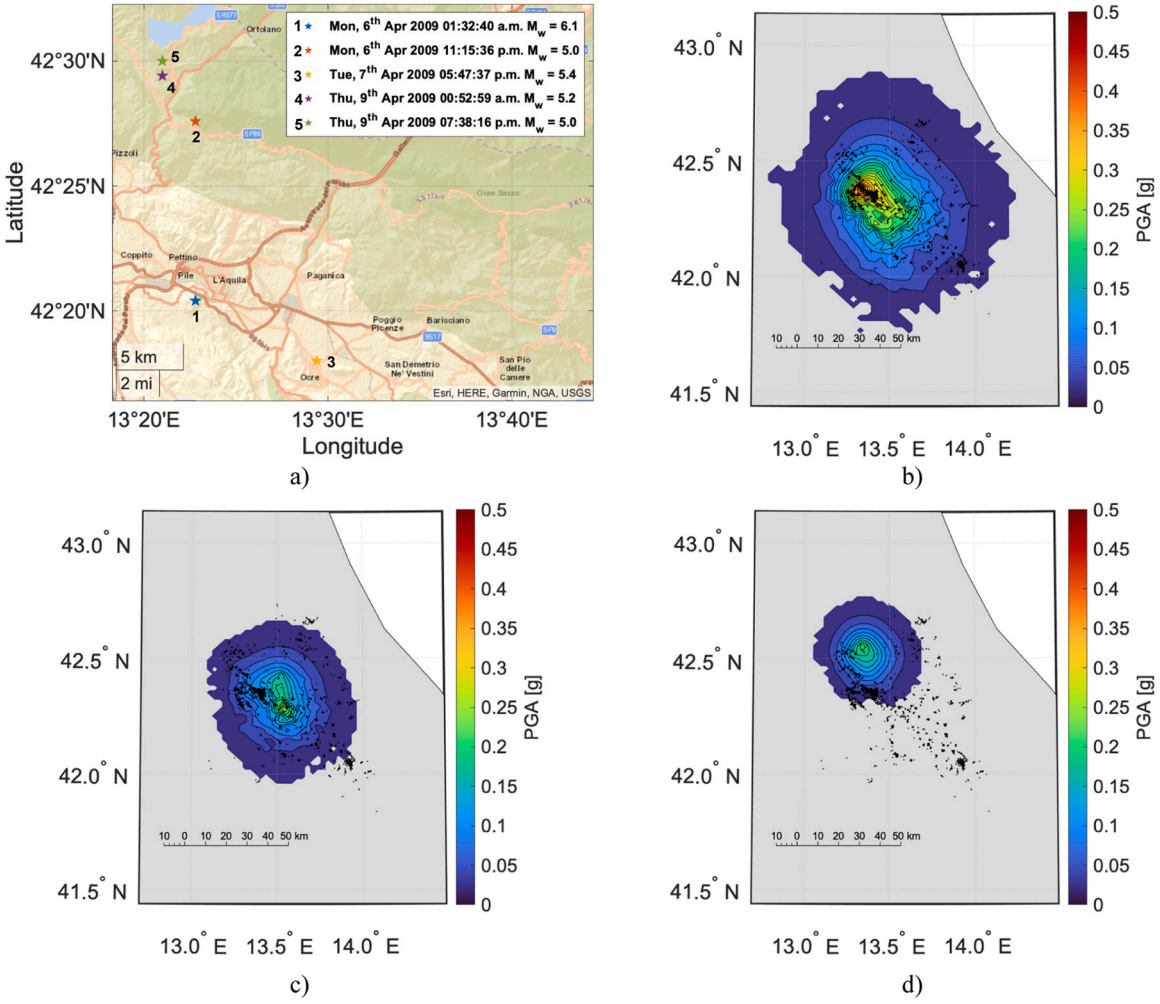

Fig. 7. (a) Epicentral sites of L'Aquila 2009 seismic sequence with $M_w \geq 5$; (b) *PGA* shake-map of the mainshock on 6th April 2009 01:32:40 a.m., $M_w = 6{,}1$; (c) *PGA* shake-map of the aftershock on 7th April 2009 05:47:37 p.m., $M_w = 5{,}4$; (d) *PGA* shake-map of the aftershock on 9th April 2009 07:38:16 p.m. $M_w = 5{,}0$.

earthquake occurred. The same census database was considered in other works, such as Zucconi, Ferlito, & Sorrentino [67,69], D'Amato et al. [14], Laguardia et al. [39]. The ISTAT census database, assumed in each municipality as reference, permits of knowing municipality-by-municipality only the material breakdown of buildings registered, while it does not report any other information (such as material type of horizontal and vertical structural elements, floor number, construction age) for defining typological classes similarly to the *AeDES* forms.

A municipality-by-municipality database completion including undamaged and not surveyed buildings may be conducted by comparing the buildings number having the *AeDES* form (i.e. surveyed after the 2009 L'Aquila earthquake) with the one reported in ISTAT [33] census database. In doing so, in each municipality the following *Completeness Ratio* r_m may be considered [14]:

$$r_m = \frac{N_{m,AeDES}}{N_{m,ISTAT}} \tag{4}$$

where m is the *m-th* municipality (1, …, 95), $N_{m,AeDES}$ and $N_{m,ISTAT}$ is the buildings number surveyed with *AeDES* form (included within *Da.D.O.* database) and during the ISTAT census, respectively.

Basically, a perfect correspondence between buildings registered during the ISTAT [33] census having also an *AeDES* form would lead in each municipality to a completeness ratio r_m ideally equal to 1. To this scope Fig. 9a reports a histogram of r_m intervals found in the municipalities analysed, while Fig. 9b illustrates the completeness ratios map. Contrary to what was expected, one may observe that in this case r_m reaches values greater than 1 in the zones around the seismic sequence epicentres, while far from the latter a r_m lower than 1 is obtained. These numerical inconsistencies are also found in other previous works, Dolce & Manfredi [19], Zucconi, Ferlito, & Sorrentino [67] and D'Amato et al., [14]. In particular, it is easy reasonable that in the municipalities where the earthquake occurred with a low intensity, almost of all undamaged buildings were hence not surveyed, so that we found $r_m < 1$ [14]. On the other hand, $r_m > 1$ may be very likely due to a different definition of "*building*" assumed by the two databases, and because of some building was not recorded during the ISTAT [33] census but surveyed with the *AeDES* form after L'Aquila 2009 earthquake [14]. This probably is due to the fact that some building was not accurately reported into the cadastral maps and, therefore, was not recorder into ISTAT census, contributing to the buildings number underestimation with respect to the *AeDES* database [67]. Lastly, it should be remembered that in this study the ISTAT [33] database is considered, since it is the closest database to the L'Aquila 2009 earthquake. Therefore, it could be possible that discrepancies between ISTAT [33] and *AeDES* database are given to the fact that some building after the L'Aquila 2009 seismic swarm was demolished and, consequently, not considered in the ISTAT census. However, this is still an open issue, needing to be investigated more in depth in the future.

In this study it is assumed that buildings not surveyed (i.e. without *AeDES* form) did not have any damage due to L'Aquila seismic sequence.

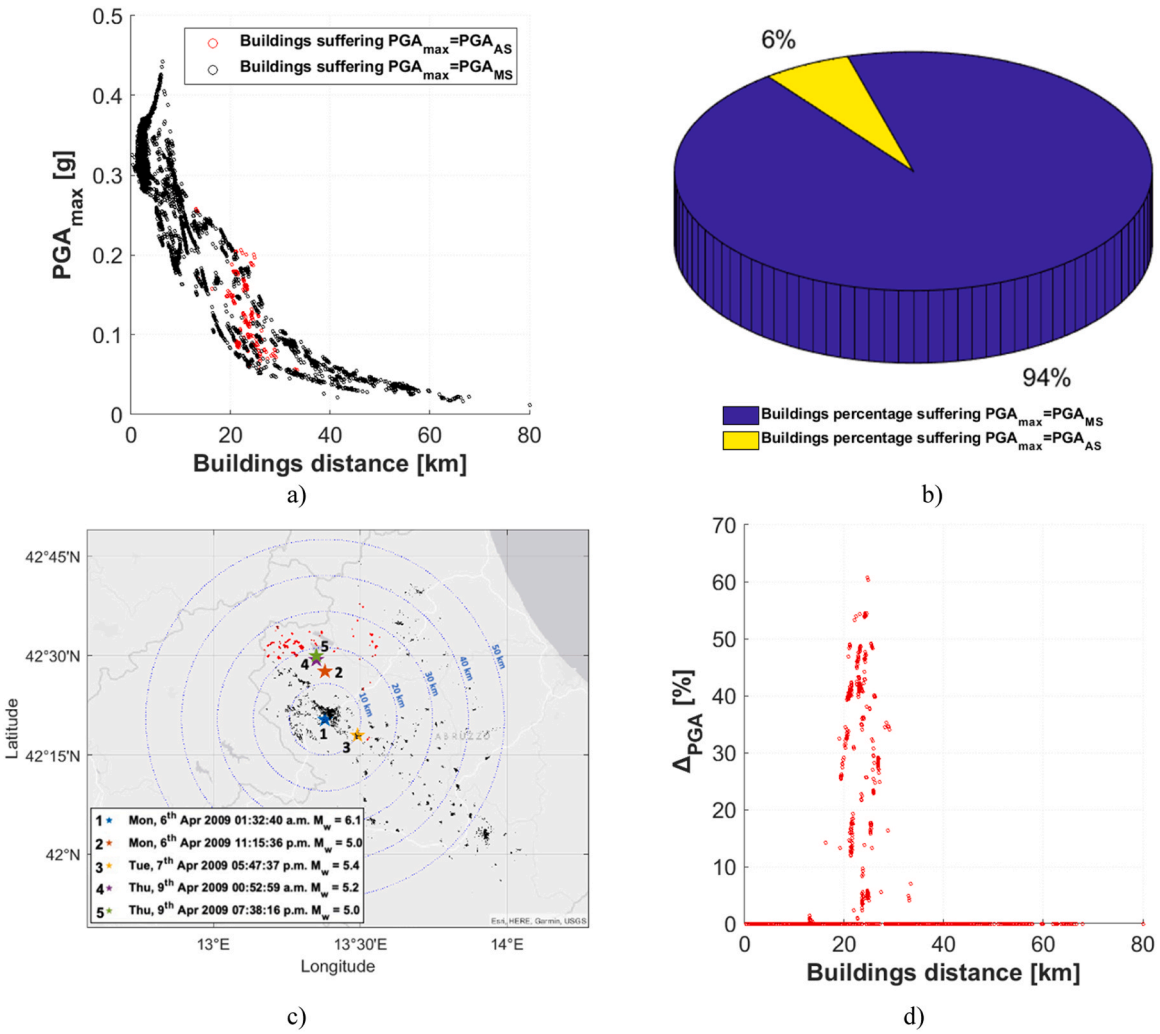

Fig. 8. (a) *PGA* values from the mainshock epicenter (6th April 2009, $M_w = 6.1$) recorded during the mainshock and the aftershocks; (b) Percent distribution of the maximum *PGA* occurred during the mainshock or aftershocks; (c) Residential buildings maps and distance from the mainshock epicenter; d) *PGA* percentage increment respect to the value recorded in the mainshock.

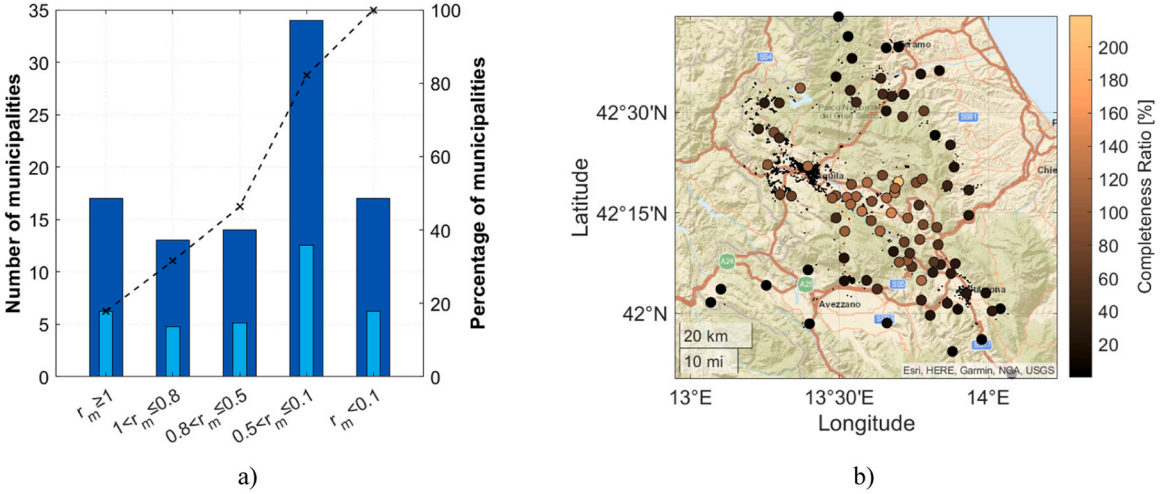

Fig. 9. (a) r_m intervals found in the 95 municipalities analyzed; (b) completeness ratios map.

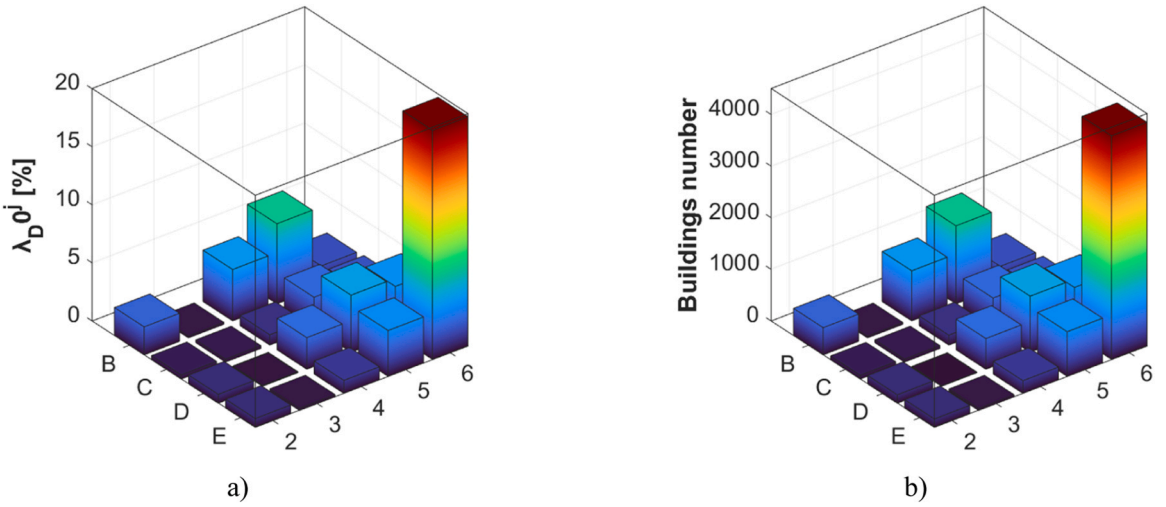

Fig. 10. *MB:1H-1V*. (a) λ_{D0}^{j} (in percentage) and (b) number of undamaged buildings added for all the structures typologies considered.

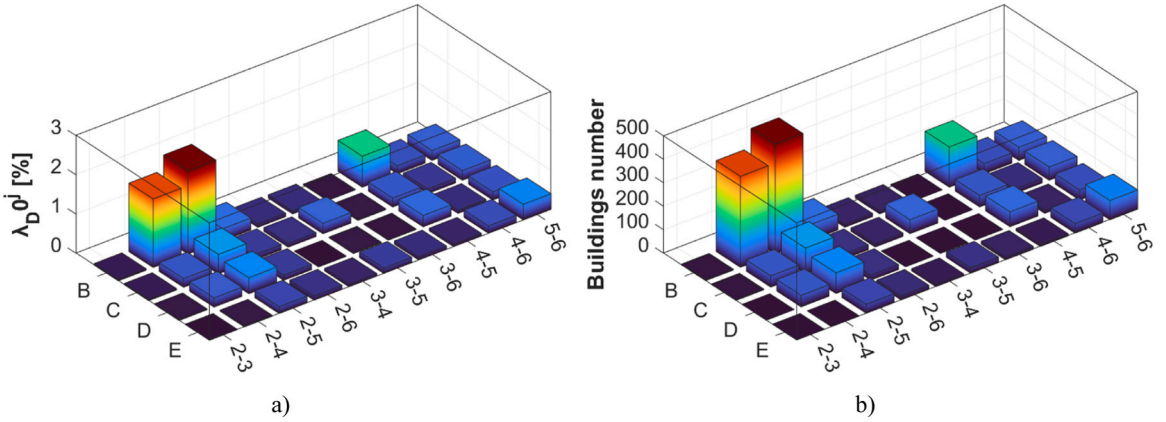

Fig. 11. *MB:2H-1V*. (a) λ_{D0}^{j} (in percentage) and (b) number of undamaged buildings added for all the structures typologies considered.

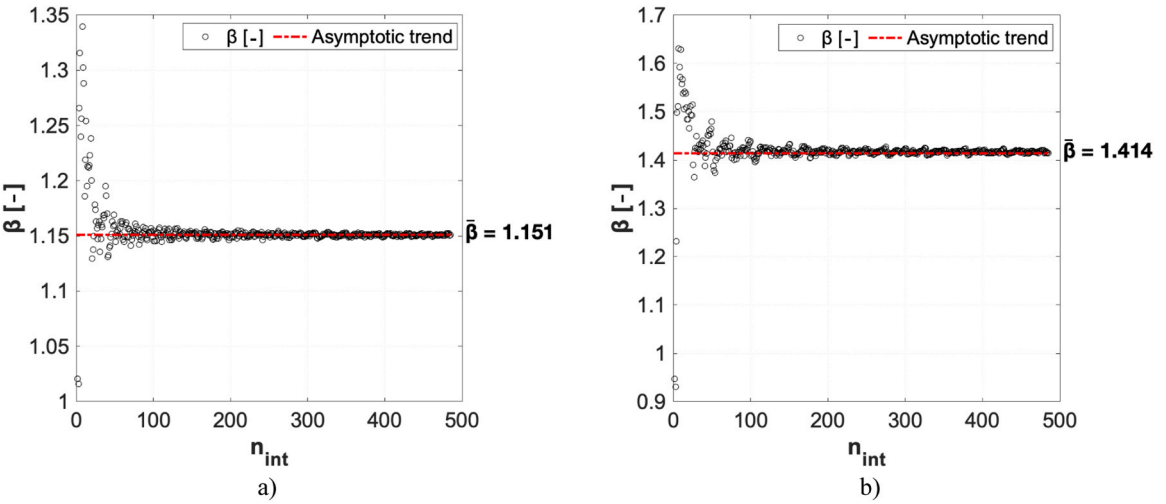

Fig. 12. Standard deviation of the *PGA* logarithmic values β. Masonry type a) *2C* and b) *2D–4D*.

Therefore, a D_0 level is assigned to these buildings. According to this assumption, in the municipalities where $r_m < 1$, the masonry residential buildings stock is completed as follows [59,60]:

$$N_{m,added}^{D0} = N_{m,ISTAT} - N_{m,AeDES}^{D0-D5} (m = 1, \ldots, 95) \quad (5)$$

where $N_{m,added}^{D0}$ is the undamaged buildings number added for completing

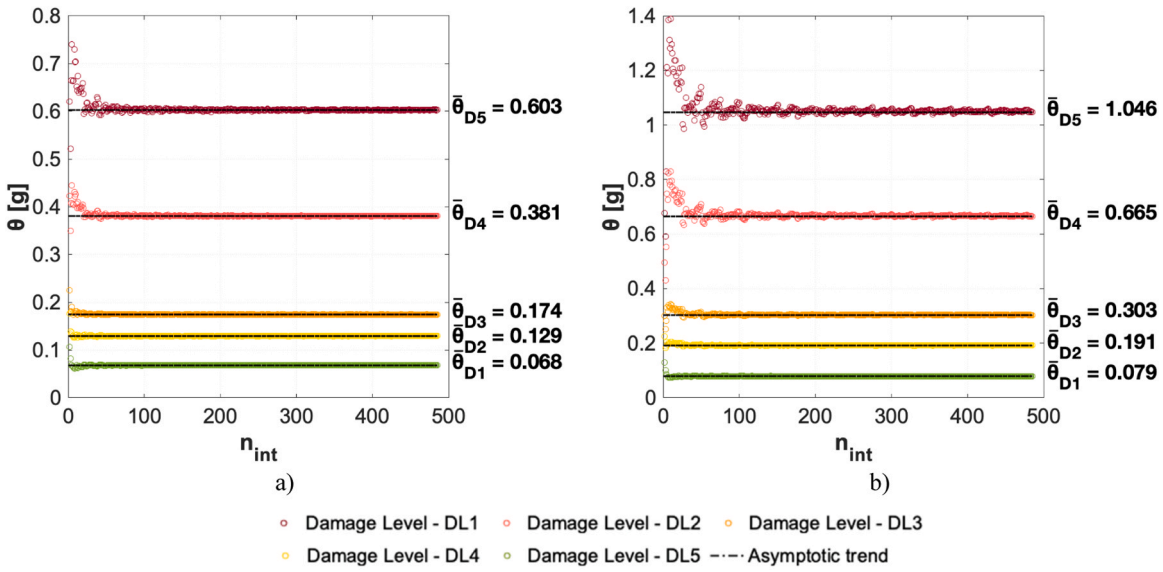

Fig. 13. Median of *PGA* values ϑ for different damages level. Masonry type (a) *2C* and (b) *2D–4D*.

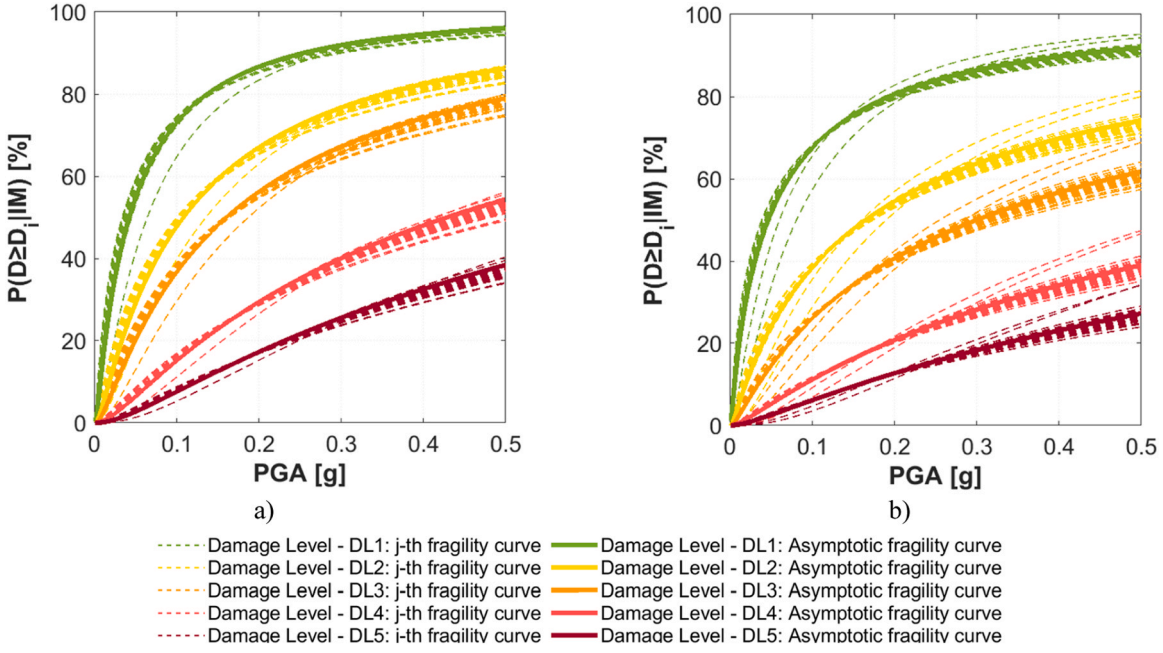

Fig. 14. Fragility curves obtained by varying $(\vartheta_{D1}, \ldots, \vartheta_{D5}, \beta)$ for several n_{int}. Masonry type (a) *2C* and (b) *2D–4D*.

the buildings stock in the *m-th* municipality, and $N_{m,AeDES}^{D0-D5}$ is the buildings number reported in the *Da.D.O.* database having an *AeDES* form. Hence, the total buildings number $N_{m,tot}$ is given by:

$$N_{m,tot} = N_{m,ISTAT} = N_{m,AeDES}^{D0-D5} + N_{m,added}^{D0} \tag{6}$$

by assuming that in each municipality the buildings distribution by construction material, and in particular for masonry buildings considered in this study, is derived from ISTAT [33] census buildings stocks.

In accordance with the assumptions made, starting from the stock of $N_{AeDES}^{D0-D5} = \sum N_{m,AeDES}^{D0-D5} = 56.338$ masonry residential buildings surveyed with *AeDES* form, the completion procedure adopted provides $N_{added} = \sum N_{m,added}^{D0} = 21.955$, yielding to a completed buildings stock of $N_{m,tot} = \sum N_{m,tot} = 78.293$ buildings.

Unfortunately, the ISTAT [33] census database does not provide any information on masonry structures typologies as appear in the *AeDES* form and reported in the Table 1, as possible combination between horizontal (indicated with a number from *1* to *6*) and vertical structural elements (indicated with a letter from *A* to *E*). Hence, in order to obtain a hypothetical undamaged buildings breakdown according to *AeDES* form typologies, it is assumed that this unknown breakdown follows the known undamaged buildings breakdown observed from the *AeDES* forms. Therefore, in the *m-th* municipality the following expression is applied for calculating the added number of undamaged buildings (i.e. with D_0) $N_{m,added}^{D0,j}$ for the *j-th* masonry structures typology (Table 1):

$$N_{m,added}^{D0,j} = \frac{\sum_{m=1}^{95} N_{m,AeDES}^{D0,j}}{\sum_{m=1}^{95} N_{m,AeDES}^{D0}} N_{m,added}^{D0} = \lambda_{D0}^{j} \bullet N_{m,added}^{D0} \tag{7}$$

where $N_{m,added}^{D0}$ is the undamaged buildings number added by means of

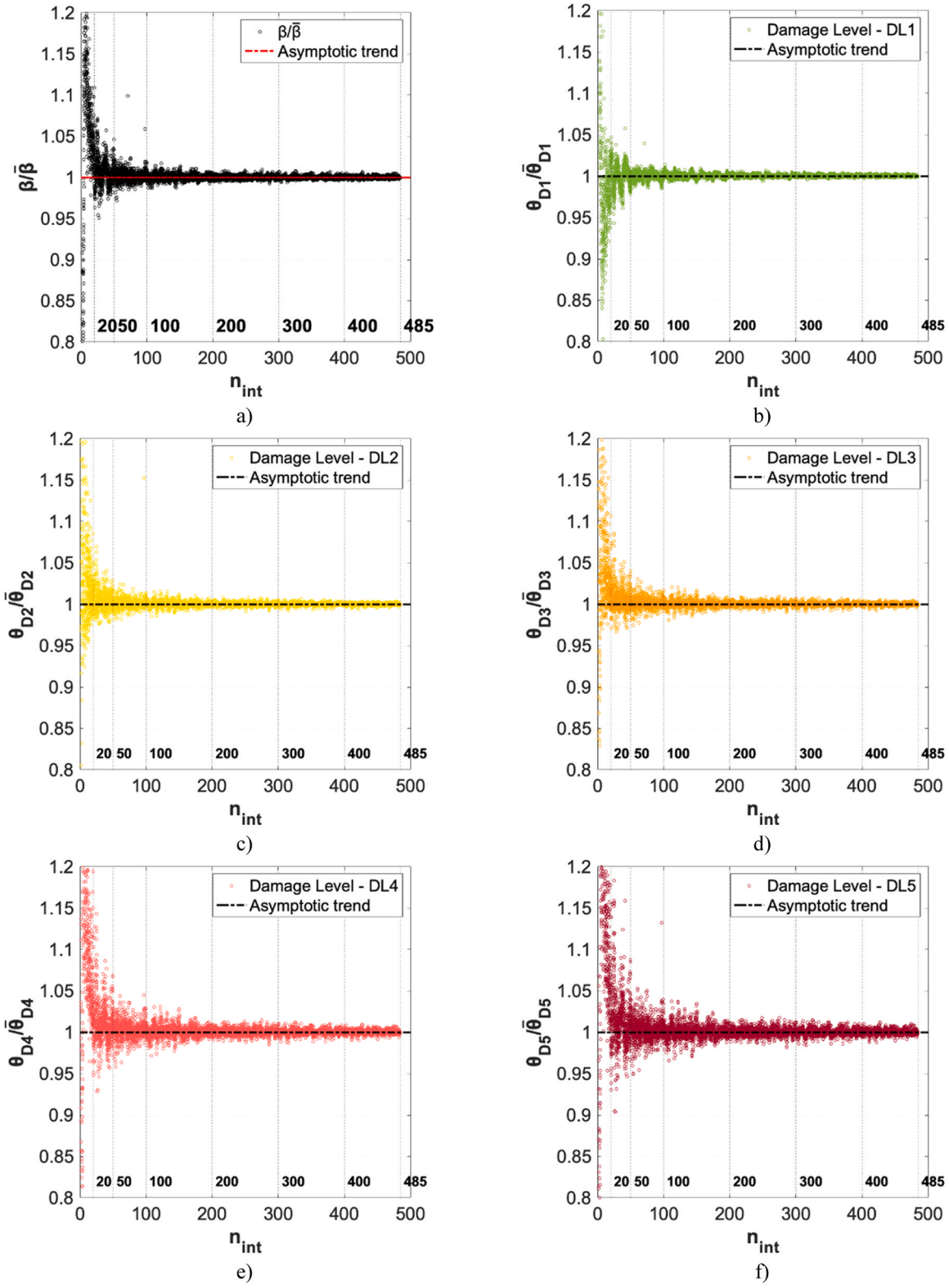

Fig. 15. Masonry residential buildings stock of L'Aquila 2009 (completed database). (a) Ratio $\beta/\bar{\beta}$; (b), (c), (d), (e) and (f) ratios $\vartheta_{Di}/\bar{\vartheta}_{Di}$.

Eq. 5; while $N_{m,AeDES}^{D0,j}$ and $N_{m,AeDES}^{D0}$ refer to the *m-th* municipality and correspond, respectively, to the undamaged buildings number belonging to the *j-th* masonry structure typology (Table 1), and to the undamaged buildings total number both with the *AeDES* form (in the case of the masonry residential buildings stock considered we found that $\sum_{m=1}^{95} N_{m,AeDES}^{D0} = 16.714$). λ_{D0}^{j} expresses, for the *j-th* masonry structure typology, the ratio between the sums of $N_{m,AeDES}^{D0,j}$ and $N_{m,AeDES}^{D0}$ referred to all the municipalities, so that $\sum_j \lambda_{D0}^{j} = 1$. In the Eq. 7 the sums are extended to all the undamaged buildings of all the 95 municipalities considered because of it is assumed that in this way a better masonry structures typologies breakdown of undamaged buildings may be estimated. However, this aspect deserves to be investigated more in detail in

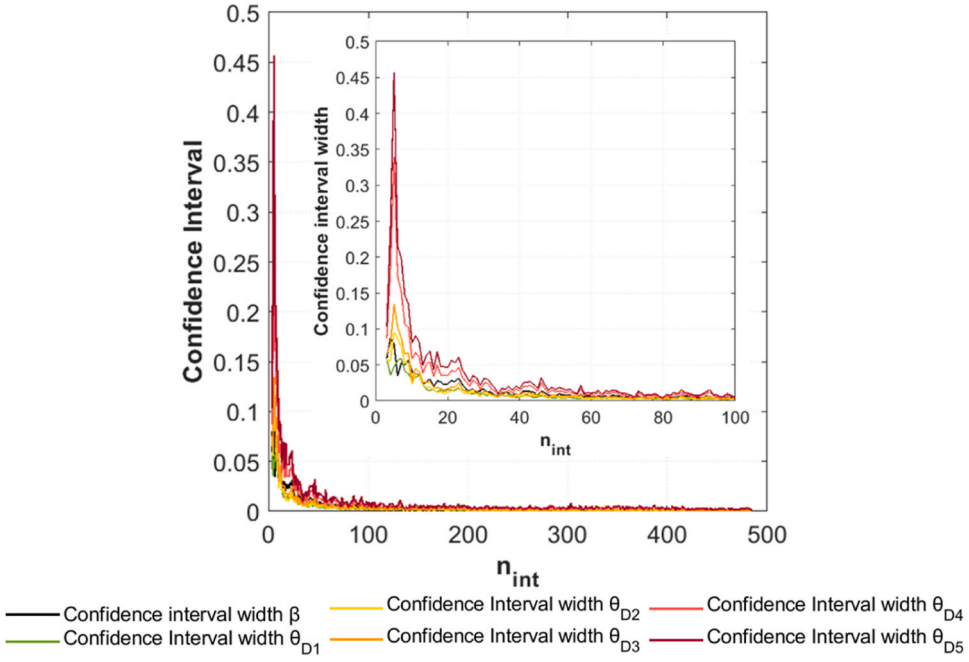

Fig. 16. Confidence Intervals of ratios $\vartheta_{Di}/\overline{\vartheta}_{Di}$ and $\beta/\overline{\beta}$ plotted in Fig. 15 at a 95% confidence level.

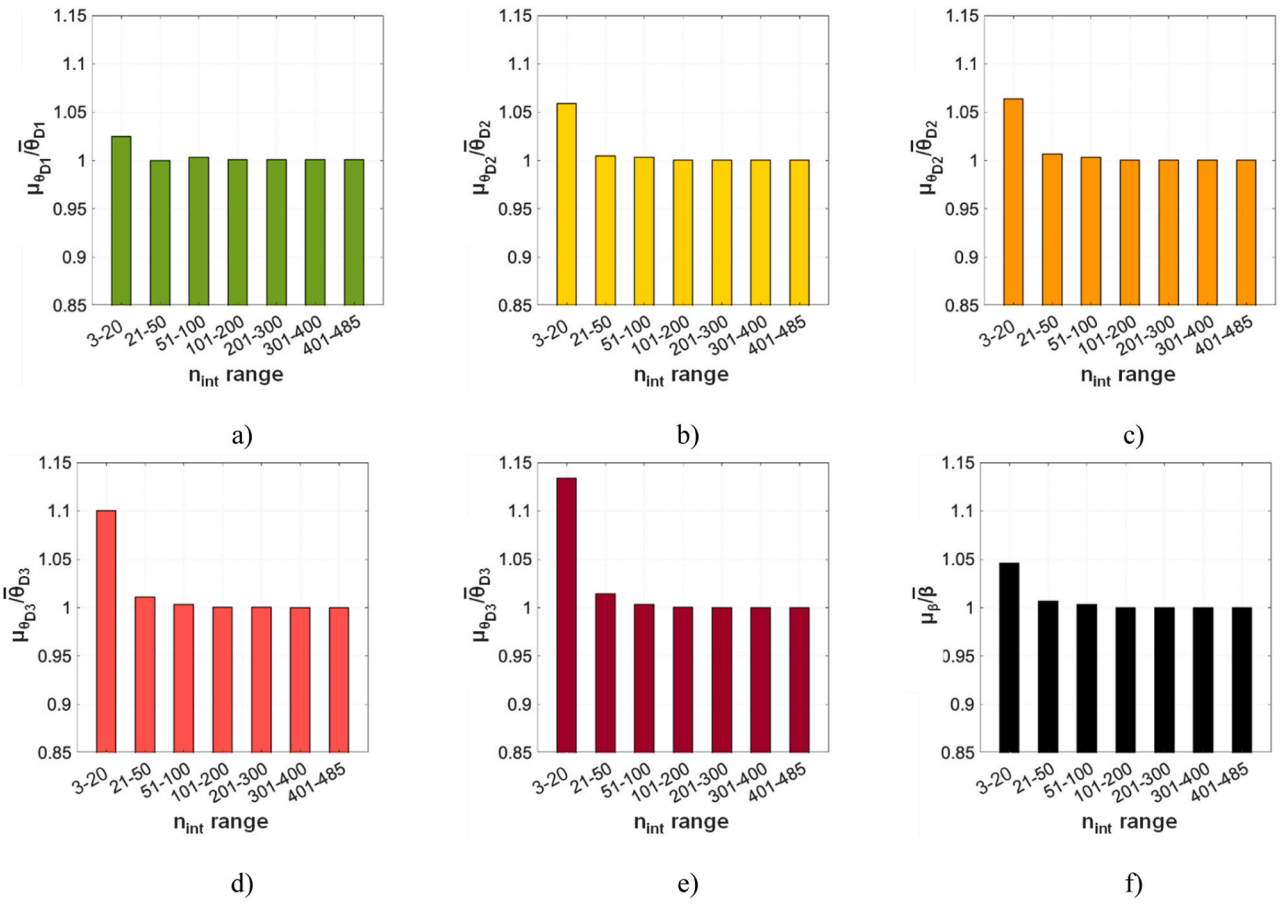

Fig. 17. Ratios (a) $\mu_{\vartheta_{D1}}/\overline{\vartheta}_{D1}$, (b) $\mu_{\vartheta_{D2}}/\overline{\vartheta}_{D2}$, (c) $\mu_{\vartheta_{D3}}/\overline{\vartheta}_{D3}$, (d) $\mu_{\vartheta_{D4}}/\overline{\vartheta}_{D4}$, (e) $\mu_{\vartheta_{D5}}/\overline{\vartheta}_{D5}$ and (f) $\mu_{\beta}/\overline{\beta}$ for several n_{int} ranges.

the future due to the uncertainties that this kind of estimation may imply. For completeness Fig. 10 and Fig. 11 report, according to the Eq. 7, for all masonry structures typologies of the Table 1 the ratio λ^{j}_{D0} (in percentage) and the number of undamaged buildings added. In particular, Fig. 10 refers to case of *MB:1H-1V* (masonry residential buildings have one horizontal and one vertical structural element); whereas

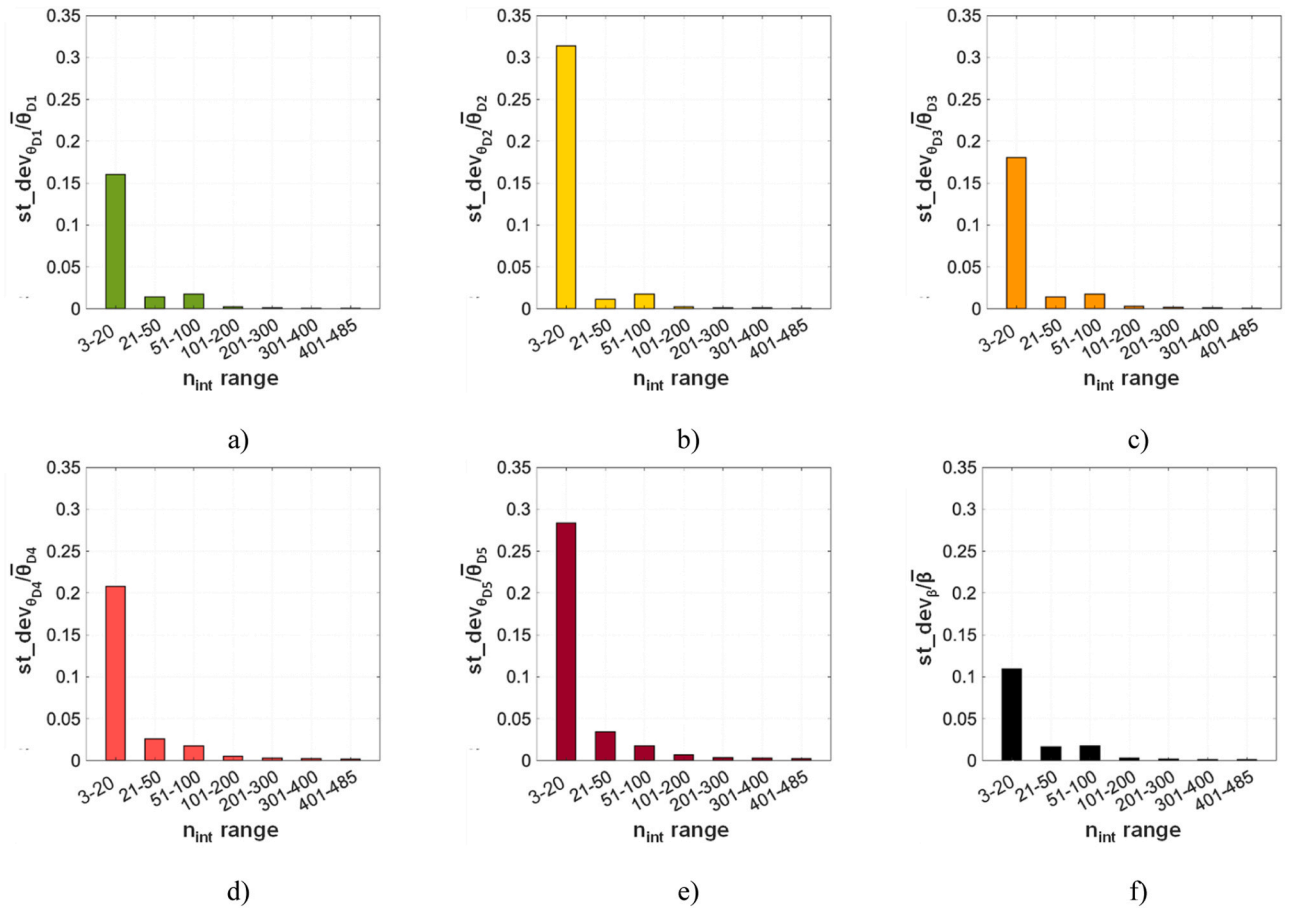

Fig. 18. Standard deviations (a) $st\_dev_{\vartheta_{D1}}/\overline{\vartheta}_{D1}$, (b) $st\_dev_{\vartheta_{D2}}/\overline{\vartheta}_{D2}$, (c) $st\_dev_{\vartheta_{D3}}/\overline{\vartheta}_{D3}$, (d) $st\_dev_{\vartheta_{D4}}/\overline{\vartheta}_{D4}$, (e) $st\_dev_{\vartheta_{D5}}/\overline{\vartheta}_{D5}$ and (f) $st\_dev_{\beta}/\overline{\beta}$ for several n_{int} ranges.

Fig. 11 plots the results obtained with respect to the *MB:2H-1V* buildings.

The procedure proposed for database completion is easy to be implemented since it requires information available from the buildings already surveyed, and from Italian national census periodically performed on the buildings stock considered. Of course, it represents a first tentative of taking into account the undamaged and not surveyed residential buildings for deriving fragility curves that may be significative from a statistic point of view. In this way, the completion proposed permits of obtaining a breakdown of the masonry undamaged buildings (added) for all the structural typologies considered by the *AeDES* form (Table 1).

6. Sample partitioning for fragility curves fitting the observed seismic damage

As previously introduced, for fitting fragility curves to the observed seismic damage of a certain buildings stock, a sample partition in *IM* intervals is necessary having in general a constant amplitude. The *j-th* interval (bin) with limits $IM_j \pm \Delta IM/2$, includes the buildings seismic damage from D_0 to D_5 [5].

Once the buildings stock seismic damage is partitioned, the *MLE* method is applied in order to estimate the fundamental parameters $(\vartheta_1, \ldots, \vartheta_5, \beta)$ describing the fragility curves for any damage level (Eq. 3) [40,5,56]. Without any doubt, the partitioning is a crucial point since how to choose the intervals number (n_{int}) and, consequently, their amplitude ΔIM influences the fundamental parameters estimation $(\vartheta_1, \ldots, \vartheta_5, \beta)$. For demonstrating this, a sensitivity analysis is performed in this study calculating the fundamental parameters by varying the *IM* intervals amplitude, by assuming in this case that *IM* corresponds to the *PGA*. Numerical investigations are referred to several typologies of masonry residential buildings belonging to the L'Aquila 2009 buildings stock available within *Da.D.O.*, and completed as proposed in this study.

As example, Fig. 12 and Fig. 13 report the fundamental parameters obtained by referring to two different masonry typologies according to *AeDES* classification (Table 1), that are: *type 2C*, i.e. buildings with masonry of irregular texture and poor quality, with tie-rods and tie-beams; *type 2D-4D*, i.e. buildings with masonry of regular texture and good quality, with two horizontal structural elements: vaults and beam with deformable slabs, both without tie-rods and tie-beams. As for the two typologies here discussed, it results a sample of 548 buildings for *type 2C*, and of 285 buildings for *type 2D–4D*. These values are greater than an indicative lower bound of 200 buildings indicated in Rossetto et al. [48] for obtaining a theoretical acceptable sample size in fragility curves analysis. Numerical investigations are conducted by increasing the intervals number n_{int} down to about 0001 g obtaining $n_{int} = 485$, since the maximum *PGA* for both the masonry typologies investigated is equal to 0485 g. More in detail, Fig. 12 reports as the standard deviation of the *PGA* logarithmic values β (Eq. 1) varies as n_{int} increases (i.e. the interval *PGA* amplitude reduces), by referring to the *type 2C* (Fig. 12a) and to *type 2D–4D* (Fig. 12b). Analogously, Fig. 13 plots the variability of *PGA* median values as n_{int} increases for *type 2C* (Fig. 13a) and for *type 2D–4D* (Fig. 13b). As one may easily note, in the masonry typologies considered the fundamental parameters $(\vartheta_1, \ldots, \vartheta_5, \beta)$ tend to stabilize as the interval number increases, reaching substantially an asymptotic value. In both the cases analysed β rapidly reduces its dispersion as n_{int} increases (Fig. 12), and tends to converge on the asymptotic values ($\overline{\beta}$) when n_{int} is higher than 100. Whereas, as for the fundamental parameter $(\vartheta_1, \ldots, \vartheta_5)$ it is observed that they soon converge on the asymptotic value for a very small value of n_{int} only for damage level D_1, D_2 and D_3

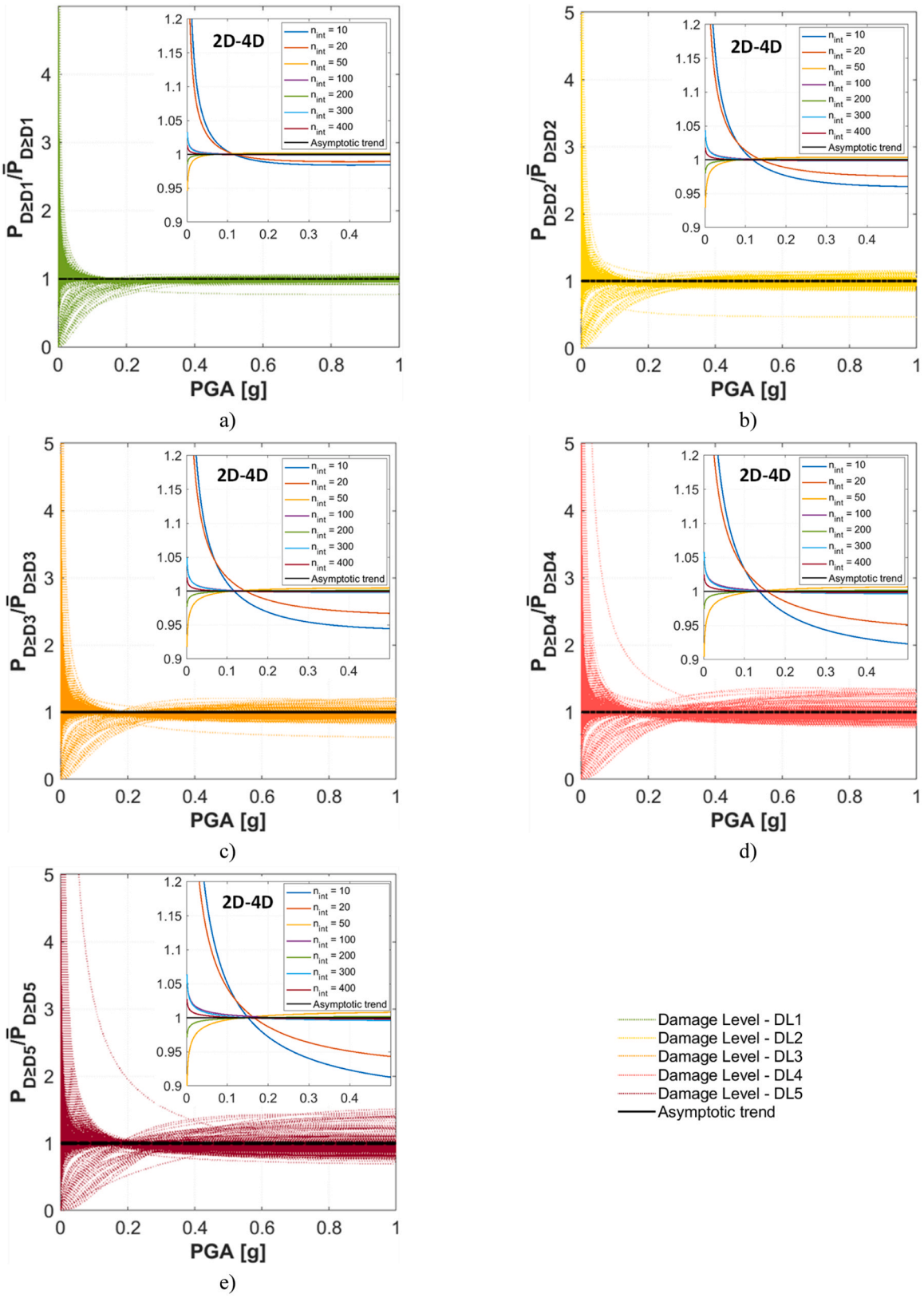

Fig. 19. Fragility curves ordinates ratios $P_{D\geq Di}/\bar{P}_{D\geq Di}$ for all the damage levels considered.

($\bar{\vartheta}_{D1}, \bar{\vartheta}_{D2}, \bar{\vartheta}_{D3}$). While, a more marked dispersion around the asymptotic values is observed in the case of D_4 and D_5 ($\bar{\vartheta}_{D4}, \bar{\vartheta}_{D5}$), stabilizing when n_{int} is higher than 100.

Finally, it is useful to understand how the fundamental parameters variability reported in Fig. 12 and Fig. 13 reflect on the corresponding fragility curves. To this aim, Fig. 14 illustrates a set of fragility curves (D_1-D_5) for *type 2C* (Fig. 14a) and *type 2D–4D* (Fig. 14b), calculated for different values of $(\vartheta_{D1}, \ldots, \vartheta_{D5}, \beta | n_{\text{int}})$ each of which related to a specific

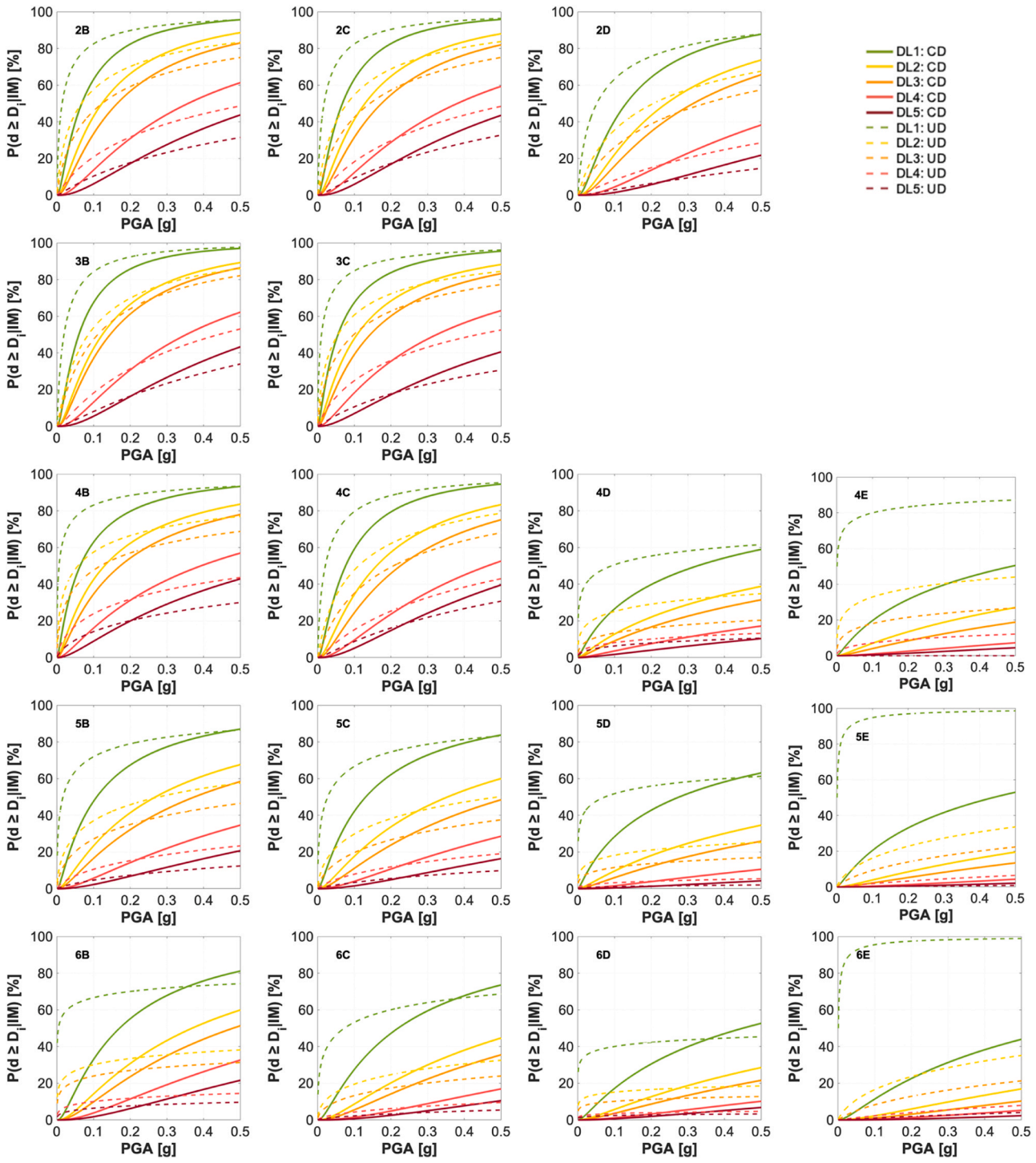

Fig. 20. *MB:1H-1V*. Typological fragility curves from *type 2B* to *type 6E* (Table 1).

n_{int}. In these graphs the thicker fragility curves indicate the ones calculated by referring to the asymptotic values highlighted in Fig. 12 and Fig. 13. As one may note the variability of $(\vartheta_{D1}, \ldots, \vartheta_{D5}, \beta | n_{int})$ reflects, of course, on the fragility curves of Fig. 14, that is less relevant in the case of masonry *type 2C* (Fig. 14a) and, on the contrary, more pronounced in the case of masonry *type 2D–4D* (Fig. 14b). Therefore, it may be concluded that reliable fragility curves are obtained if a non-arbitrary *PGA* intervals number (n_{int}) is chosen. In the cases analysed n_{int} results equal to about 100.

The fundamental parameters convergence discussed in detail for the masonry *types 2C* and *2D–4D* may be generalized for all other residential masonry types considered in this study. This is proved in Fig. 15 plotting the dimensionless ratios $\vartheta_{Di}/\overline{\vartheta}_{Di}$ (i = 1, …, 5) and $\beta/\overline{\beta}$ referred to all the Table 1 typologies where it has been possible to derive ϑ_{Di} and β for all the damage levels. The asymptotic values $\overline{\vartheta}_{Di}$ and $\overline{\beta}$ are generally found when 485 intervals are considered. As it is easy to note, although a certain dispersion is observed when the n_{int} is low, dimensionless ratios tend to the unity when n_{int} is 100 or higher, even if a monotonic convergence is not observed. Fig. 16 depicts an estimation of the interval width computed at 95% confidence level for each of the dimensionless ratios $\vartheta_{Di}/\overline{\vartheta}_{Di}$ (i = 1, …, 5) and $\beta/\overline{\beta}$. The interval width is obtained as upper bound – lower bound, and plotted by varying n_{int}. In this way it is

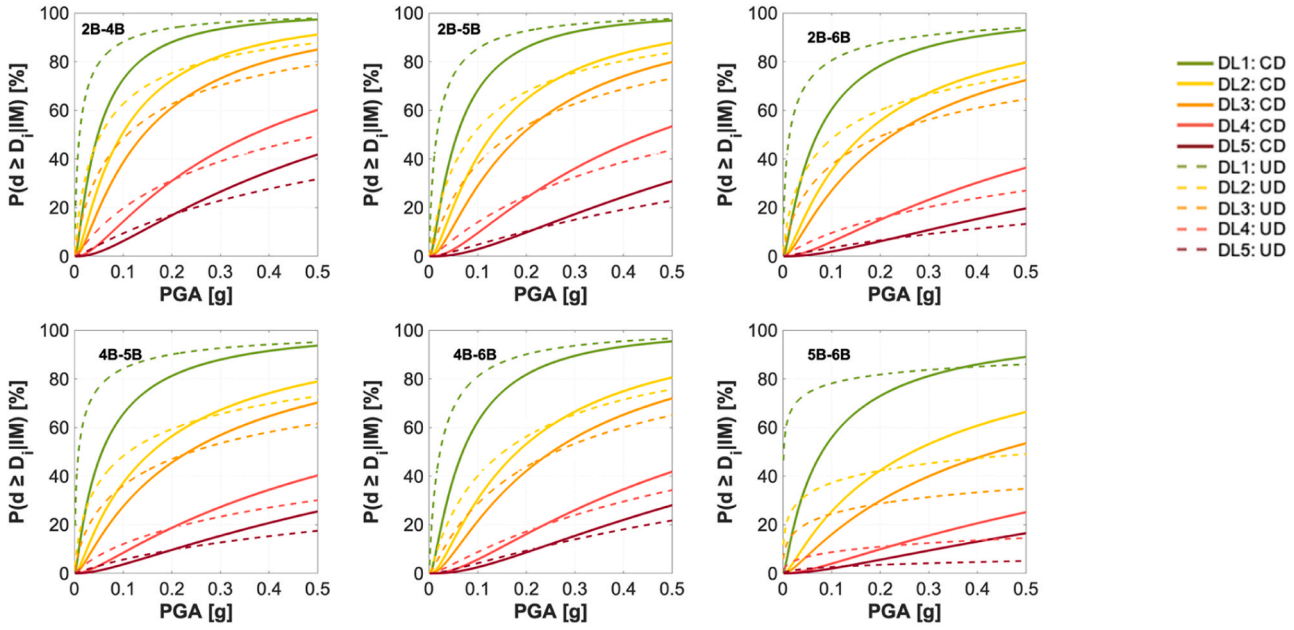

Fig. 21. *MB:2H-1V*. Typological fragility curves of *type B* (Table 1).

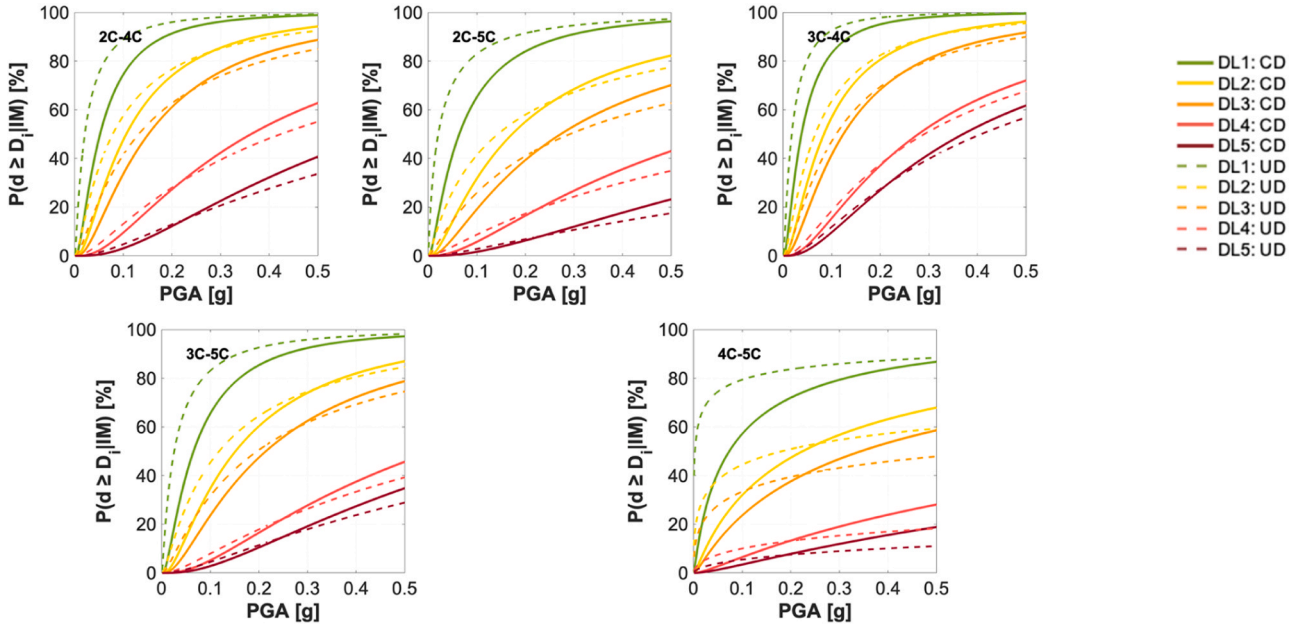

Fig. 22. *MB:2H-1V*. Typological fragility curves of *type C* (Table 1).

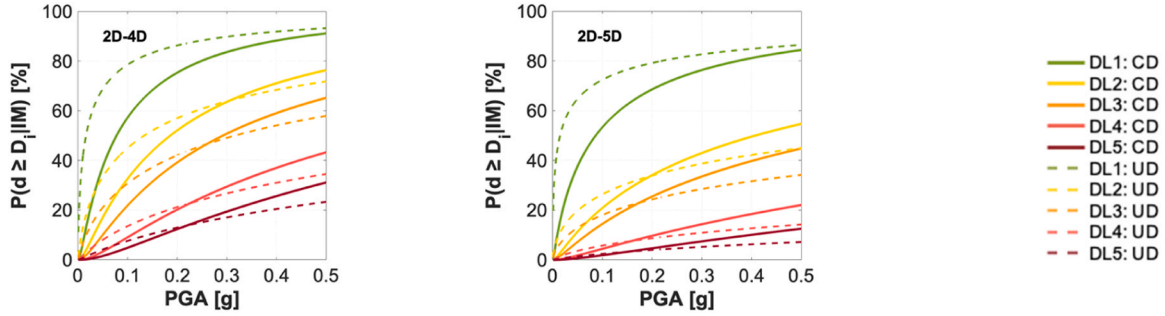

Fig. 23. *MB:2H-1V*. Typological fragility curves of *type D* (Table 1).

Table 4
MB:1H-1V. Fundamental parameters of fragility curves from *type 2B* to *type 6E* (Table 1).

type	n.	$\overline{\vartheta}_{D1}$ [g]	$\overline{\vartheta}_{D2}$ [g]	$\overline{\vartheta}_{D3}$ [g]	$\overline{\vartheta}_{D4}$ [g]	$\overline{\vartheta}_{D5}$ [g]	β [-]
2B	3.890	0,068	0,123	0,164	0,357	0,600	1,164
2C	548	0,068	0,123	0,174	0,381	0,603	1,151
2D	712	0,132	0,241	0,315	0,704	1,222	1,147
3B	260	0,060	0,124	0,145	0,352	0,604	1,125
3C	404	0,056	0,108	0,143	0,324	0,681	1,296
4B	6.982	0,064	0,130	0,173	0393	0,640	1,378
4C	1.254	0,077	0,161	0,226	0,463	0,682	1,172
4D	2.228	0,326	0,854	1,240	2980	5,388	1,884
4E	831	0,488	1,559	2,584	7,473	11,687	1,856
5B	7.663	0,108	0,269	0,375	0,856	1,513	1,356
5C	2.645	0,131	0,354	0,527	1,078	1,890	1,358
5D	4.014	0,276	1,008	1,573	4,587	10,496	1,772
5E	2.969	0,437	2,313	3,583	10,632	18,811	1,783
6B	1.609	0,171	0,368	0,480	0,865	1,299	1,216
6C	1.624	0,219	0,596	0,813	1,751	2,576	1,308
6D	3.084	0,450	1,229	1,741	3,759	5,334	1,587
6E	13.645	0,631	2,155	3,433	5,961	10,495	1,524

Table 5
MB:2H-1V. Fundamental parameters of fragility curves of *type B* (Table 1).

type	n.	$\overline{\vartheta}_{D1}$ [g]	$\overline{\vartheta}_{D2}$ [g]	$\overline{\vartheta}_{D3}$ [g]	$\overline{\vartheta}_{D4}$ [g]	$\overline{\vartheta}_{D5}$ [g]	β [-]
2B–4B	3.705	0,048	0,097	0,142	0,365	0,641	1,213
2B–5B	3.782	0,058	0,130	0,190	0,452	0,890	1,156
2B–6B	425	0,071	0,165	0,226	0,794	1,554	1,331
4B–5B	1.207	0,057	0,159	0,234	0,710	1,280	1,426
4B–6B	271	0,069	0,182	0,253	0,637	0,988	1,172
5B–6B	308	0,081	0,267	0,439	1,354	2,124	1,487

Table 6
MB:2H-1V. Fundamental parameters of fragility curves of *type C* (Table 1).

type	n.	$\overline{\vartheta}_{D1}$ [g]	$\overline{\vartheta}_{D2}$ [g]	$\overline{\vartheta}_{D3}$ [g]	$\overline{\vartheta}_{D4}$ [g]	$\overline{\vartheta}_{D5}$ [g]	β [-]
2C-4C	481	0,052	0,106	0,152	0,363	0,630	0,983
2C-5C	742	0,064	0,173	0,273	0,611	1,156	1,146
3C-4C	246	0,038	0,084	0,124	0,279	0,371	1,003
3C-5C	402	0,066	0,152	0,214	0,561	0,756	1,059
4C-5C	283	0,074	0,224	0,344	1,354	2,278	1,719

Table 7
MB:2H-1V. Fundamental parameters of fragility curves of *type D* (Table 1).

type	**n.**	$\overline{\vartheta}_{D1}$ **[g]**	$\overline{\vartheta}_{D2}$ **[g]**	$\overline{\vartheta}_{D3}$ **[g]**	$\overline{\vartheta}_{D4}$ **[g]**	$\overline{\vartheta}_{D5}$ **[g]**	**β [-]**
2D–4D	285	0,078	0,186	0,292	0,631	0,984	1,377
2D–5D	479	0,087	0,407	0,627	1,897	3,649	1,733

possible to note that the confidence interval width rapidly reduces to zero as n_{int} increases, despite the high confidence level (95%).

Fig. 17 and Fig. 18 illustrate, in a different way, what depicted in Fig. 15. In particular, Fig. 17a reports the ratio $\mu_{\vartheta_{D1}}/\overline{\vartheta}_{D1}$, where $\mu_{\vartheta_{D1}}$ is the mean of the fundamental parameters ϑ_{D1} (median value) calculated in each n_{int} range (bin) considered (such as *3–20*, *21–50*, *51–100*, *101–200*, *201–300*, *301–400* and *401–485*), and $\overline{\vartheta}_{D1}$ is the corresponding asymptotic value. Similarly, the ratios $\mu_{\vartheta_{D2}}/\overline{\vartheta}_{D2}$-$\mu_{\vartheta_{D5}}/\overline{\vartheta}_{D5}$ of other damage levels are plotted in Fig. 17b-e. Finally, Fig. 17f reports the ratio $\mu_{\beta}/\overline{\beta}$, where μ_{β} is the mean of the fundamental parameters β (logarithmic standard deviation) calculated in each n_{int} range considered, and $\overline{\beta}$ is the asymptotic value found. Fig. 18a reports the ratio $st\_dev_{\vartheta_{D1}}/\overline{\vartheta}_{D1}$, where $st\_dev_{\vartheta_{D1}}$ is the standard deviation of the fundamental parameters ϑ_{D1} (median value) resulting in each n_{int} range (bin) considered. Analogously, Fig. 18b-e illustrate the ratios $st\_dev_{\vartheta_{D2}}/\overline{\vartheta}_{D2}$-$st\_dev_{\vartheta_{D5}}/\overline{\vartheta}_{D5}$, respectively. Whereas, Fig. 18f shows the ratio $st\_dev_{\beta}/\overline{\beta}$, where st_dev_{β} is the standard deviation of the fundamental parameters β (logarithmic standard deviation) calculated in each n_{int} range considered. It is easy to observe that, for all the masonry typologies considered, as the n_{int} increases the mean value of the ratios $\vartheta_{Di}/\overline{\vartheta}_{Di}$ and $\beta/\overline{\beta}$ converge to 1, whereas their standard deviations reduce to zero. This permits to generalize the results previously obtained for the two specific masonry residential typologies considered (masonry *type 2C* and *2D–4D*, Fig. 12 through Fig. 14). Therefore, a rapid converge on the asymptotic values of the fundamental parameters ϑ_{Di} and β may be expected by increasing the *PGA* intervals number. Finally, Fig. 19 illustrates, for all typologies of Table 1, the ratios $P_{D\geq Di}/\overline{P}_{D\geq Di}$, where $P_{D\geq Di}$ is the fragility curve ordinate by referring to $(\vartheta_{D1},\ldots,\vartheta_{D5},\beta|n_{\text{int}})$, and $\overline{P}_{D\geq Di}$ the corresponding fragility curve ordinate referred to the asymptotic values $(\overline{\vartheta}_{D1},\ldots,\overline{\vartheta}_{D5},\overline{\beta})$. For clarity also curves referred to only some n_{int} are reported in a different scale (such as 10, 20, 50, 100, 200, 300 and 400), too. For brevity, these graphs are illustrated by considering only the masonry residential typology *2D–4D*. It is easy to note that, even if a monotonic convergence is not observed again, the ratios tend clearly to the unity, with a greater dispersion for low *PGA* values for all the damage levels.

7. Typological fragility curves proposed

In order to derive typological fragility curves for several residential masonry buildings typologies (according to the Table 1 classification), a municipality-by-municipality database completion of the buildings stock is applied, by means of the approach indicated in Sect. 5. The resulting fragility curves are plotted in Figs. 20–23, considering the fundamental parameters equal to the obtained asymptotic values $(\overline{\vartheta}_{D1},\ldots,\overline{\vartheta}_{D5},\overline{\beta})$ summarized in Tables 4–7.

It should be noted that in order to assign to a generic building one of the typologies considered in this study a building knowledge is necessarily required. This can be done through a building visual inspection, preceded by an interview with the owner, in order to find out information such as construction age, materials, structural type and the presence (or not) of interventions occurred over the years. Furthermore, if necessary, in situ investigations may be carried out, addressed to the acquisition of information necessary to be able to identify the typology consistent with one of those defined in Baggio et al. [4]. By the contrast, if some information is insufficient or missing to identify vertical and horizontal structural elements, a correct typology may not be assigned and, consequently, the building should be classified as "*unidentified*" (*type A*) within *AeDES* form.

More in detail, Fig. 20 and the Table 1 illustrates the fragility curves e fundamental parameters related to the *MB:1H-1V* (Table 1), respectively. Whereas, as for *MB:2H-1V*, three typologies of vertical structures are considered that are: *type B* of Table 1 (masonry with irregular texture and poor quality without tie-rods and tie-beams), *type C* (masonry with irregular texture and poor quality with tie-rods and tie-beams), and *type D* (masonry with regular texture and good quality without tie-rods and tie-beams). They are illustrated, respectively, in Figs. 21–23 and Tables 5–7.

Lilliefors test is used to quantify the goodness of fit of the fragility curves for all the structural typologies considered [41]. This test is carried out to assess the acceptability of the lognormal distribution for a 95% confidence level as required by *ATC-58* [42,43]. The *D* statistic is the *Kolmogorov-Smirnov test* parameter corresponding to the maximum of the absolute value of the differences between the empirical and theoretical function. The null hypothesis, H_0, for the test is the decision on whether to accept or reject the hypothesis. The null hypothesis is accepted if *D* is less than or equal to *Lilliefors test* parameter D_{crit} at 5% significance level. The obtained results are presented in Table 8, and it is depicting that all the proposed fragility curves pass the *Lilliefors test* for all damage levels considered. The *D* statistic is performed by considering the asymptotic values of the fundamental parameters.

Table 8
Lilliefors test results based on asymptotic values.

type	Damage D_1		Damage D_2		Damage D_3		Damage D_4		Damage D_5		H_0
	D	D_{crit}	D	D_{crit}	D	D_{crit}	D	D_{crit}	D	D_{crit}	
2B	0,124	0,140	0,116	0,131	0,168	0,131	0,153	0,134	0,131	0,135	Accepted
2C	0,125	0,138	0,111	0,122	0,122	0,123	0,126	0,144	0,130	0,164	Accepted
2D	0,118	0,120	0,117	0,135	0,135	0,146	0,164	0,188	0,205	0,262	Accepted
3B	0,185	0,188	0,161	0,176	0,150	0,176	0,201	0,207	0,189	0,251	Accepted
3C	0,132	0,145	0,114	0,137	0,124	0,135	0,141	0,152	0,138	0,192	Accepted
4B	0,137	0,164	0,164	0,164	0,140	0,164	0,153	0,167	0,166	0,167	Accepted
4C	0,131	0,132	0,109	0,131	0,132	0,134	0,138	0,142	0,152	0,156	Accepted
4D	0,070	0,146	0,109	0,150	0,107	0,156	0,171	0,173	0,168	0,196	Accepted
4E	0,128	0,146	0,137	0,159	0,167	0,192	0,233	0,288	0,209	0,343	Accepted
5B	0,121	0,144	0,129	0,140	0,132	0,144	0,132	0,146	0,143	0,152	Accepted
5C	0,134	0,192	0,127	0,192	0,122	0,192	0,200	0,207	0,175	0,242	Accepted
5D	0,132	0,207	0,181	0,213	0,179	0,213	0,221	0,233	0,234	0,262	Accepted
5E	0,095	0,170	0,158	0,180	0,128	0,192	0,159	0,251	0,228	0,343	Accepted
6B	0,102	0,113	0,103	0,121	0,123	0,127	0,109	0,170	0,130	0,188	Accepted
6C	0,083	0,133	0,135	0,142	0,160	0,148	0,198	0,188	0,214	0,226	Accepted
6D	0,122	0,161	0,153	0,170	0,137	0,173	0,200	0,207	0,235	0,242	Accepted
6E	0,096	0,159	0,160	0,167	0,173	0,176	0,154	0,207	0,155	0,251	Accepted
2B–4B	0,162	0,184	0,179	0,184	0,146	0,184	0,165	0,180	0,146	0,176	Accepted
2B–5B	0,241	0,242	0,174	0,242	0,154	0,233	0,150	0,233	0,192	0,233	Accepted
2B–6B	0,145	0,164	0,163	0,164	0,175	0,176	0,148	0,233	0,227	0,304	Accepted
4B–5B	0,119	0,173	0,150	0,161	0,141	0,161	0,159	0,176	0,205	0,213	Accepted
4B–6B	0,154	0,170	0,167	0,180	0,178	0,192	0,212	0,324	0,184	0,324	Accepted
5B–6B	0,147	0,167	0,168	0,176	0,166	0,184	0,244	0,251	0,281	0,304	Accepted
2C-4C	0,146	0,161	0,122	0,142	0,100	0,146	0,141	0,161	0,182	0,213	Accepted
2C-5C	0,123	0,127	0,109	0,124	0,113	0,124	0,148	0,173	0,174	0,242	Accepted
3C-4C	0,185	0,207	0,173	0,176	0,185	0,196	0,180	0,219	0,207	0,233	Accepted
3C-5C	0,170	0,170	0,146	0,159	0,148	0,167	0,247	0,252	0,287	0,304	Accepted
4C-5C	0,164	0,176	0,155	0,180	0,165	0,192	0,246	0,304	0,219	0,343	Accepted
2D–4D	0,172	0,188	0,177	0,192	0,178	0,219	0,168	0,242	0,310	0,324	Accepted
2D–5D	0,124	0,152	0,124	0,167	0,146	0,188	0,219	0,288	0,287	0,343	Accepted

For sake of completeness the fragility curves plotted in Figs. 20–23 refer to both the *Completed Database* (*CD*) according to the procedure proposed in this study (continuous lines in the graphs), and the *Uncompleted Database* (*UD*, dashed lines). One may note that the database completion leads to different fragility curves for all the typological classes considered. A significant scatter is obtained demonstrating the statistical importance of the undamaged (i.e., buildings with D_0) and not surveyed buildings when fragility curves are derived. The completion with undamaged buildings influences the fragility curves with respect to both the damage level and *IM* (in this case *PGA*). For all the structural typologies considered, it is noted that the fragility curves related to the damage level D_1 lead always to overestimate the exceedance probability if the *UD* is considered. This is due to the fact that when completion is applied to the stock considered, the undamaged buildings number increases (*CD*) and, therefore, the exceedance probability of the damage level D_1 tends to reduce with respect to the case when only surveyed buildings are considered (*UD*). For the others damage levels, this overestimation arises mainly for low *PGA* values. As the *PGA* increases the scatter between the *UD* and *CD* fragility curves tend to reduce, demonstrating that the completion for high damage level and high *PGA* values is not significant, since in these cases seismic damages surveyed are dominant and, therefore, the completion becomes less relevant.

8. Conclusions

In this paper, typological fragility curves have been proposed for existing residential masonry buildings, through the macro-seismic approach by examining damage observed on a stock of 56.338 buildings affected by L'Aquila 2009 seismic sequence. They refer to the possible combinations of vertical and horizontal structural elements as contemplated within the *AeDES* form (Table 1). All the curves the fragility curves proposed, according to the *ATC-58* criterion, pass the *Lilliefors test* for all damage levels considered with a 95% confidence level.

The issues investigated may be useful in order to reduce uncertainties in deriving fragility curves. A criterion has been proposed for completing the buildings stock considered with undamaged and not surveyed buildings, that can be easily extended to any type of buildings stock. This aspect becomes particularly important in the municipalities far from the epicentre, where usually post-earthquake surveys are not uniformly conducted. Therefore, there is a lack of information on a large number of undamaged buildings, due to the fact the *AeDES* form for these buildings is not available. Comparisons among the completed and uncompleted database highlight the statistical importance of undamaged buildings added. In particular, it has been noted that for all typologies considered, the completion is particularly important for low values of damage levels and of *PGA*. While, it tends to decrease as the *PGA* increases, showing that for high damage levels and high *PGA*, database completion becomes less relevant.

Moreover, investigations have been carried out in order to evaluate the influence of the buildings stock damage partitioning on the typological fragility curves. The results obtained have demonstrated that the fundamental parameters derived by means of *MLE* method strictly depends on the *PGA* internals amplitude. Even if a non-monotonic converge is observed, they tend to stabilize as the intervals number (n_{int}) increases, converging on the asymptotic values. In the cases analysed, fundamental parameters values close to the asymptotic ones have been obtained when n_{int} is greater than 100.

Finally, in future in continuity with this work, uncertainties on the *PGA* estimation derived from shake-maps will be taken into account, in order to improve the fragility curves proposed. Moreover, other *IMs* will be also considered (*PGV*).

CRediT authorship contribution statement

All authors contributed equally to this manuscript.

Declaration of Competing Interest

The authors declare that they received no funds, grants or other

support during the preparation of this manuscript and have no financial, or non-financial, interests to disclose.

Data availability

Data will be made available on request.

References

[1] Angeletti, P., Baratta, A., Bernardini, A., Ceccotti, C., Cherubini, A., Colozza, R., Decanini, L., Diotallevi, P., Di Pasquale, G., Dolce, M., & et al. (2002). Valutazione e riduzione della vulnerabilità sismica degli edifici, con particolare riferimento a quelli strategici per la protezione civile. *Rapporto Finale Dipartimento Protezione Civile – Ufficio Servizio Sismico Nazionale, Roma*. (In Italian).

[2] Audisio L, D'Amato M, Gigliotti R. Influence of bond-slip on numerical fragility curves of RC structural columns. Procedia Struct Integr 2023;44:235–42. https://doi.org/10.1016/j.prostr.2023.01.031.

[3] Augenti N, Parisi F. Learning from construction failures due to the 2009 L'Aquila, Italy, earthquake. J Perform Constr Facil 2010;24(6):536–55. https://doi.org/10.1061/ASCECF.1943-5509.0000122.

[4] Baggio, C., Bernardini, A., Colozza, R., Corazza, L., Di Pasquale, G., Dolce, M., Goretti, A., Martinelli, A., Orsini, G., Papa, F., & Zuccaro, G. (2007). Field Manual for post-earthquake damage and safety assessment and short-term countermeasures (AeDES). *In:* A. Pinto and F. Taucer (Eds). *Translation from Italian: A. Goretti and M. Rota, JRC Scientific and Technical Reports, EUR 22868 EN-2007*. ⟨http://ipsc.jrc.ec.europa.eu⟩.

[5] Baker JW. Efficient analytical fragility function fitting using dynamic structural analysis. Earthq Spectra 2015;31(1):579–99. https://doi.org/10.1193/021113EQS025M.

[6] Baltzopoulos G, Baraschino R, Iervolino I, Vamvatsikos D. SPO2FRAG: software for seismic fragility assessment based on static pushover. Bull Earthq Eng 2017;15(10):4399–425. https://doi.org/10.1007/s10518-017-0145-3.

[7] Biglari M, Formisano A. Damage probability matrices and empirical fragility curves from damage data on masonry buildings after Sarpol-e-Zahab and bam earthquakes of Iran. Front Built Environ 2020;6. https://doi.org/10.3389/fbuil.2020.00002.

[8] Braga, F., Dolce, M., & Liberatore, D. (1982). Southern Italy November 23, 1980 earthquake: A statistical study on damaged buildings and an ensuing review of the MSK-76 scale. *In: Proceedings of the 7th European Conference on Earthquake Engineering. September 1982, Atene; CNR-PFG*. 503, Rome.

[9] Chieffo N, Formisano A. Comparative seismic assessment methods for masonry building aggregates: a case study. Front Built Environ 2019;5. https://doi.org/10.3389/fbuil.2019.00123.

[10] Chieffo N, Formisano A. The influence of geo-hazard effects on the physical vulnerability assessment of the built heritage: an application in a district of Naples. Buildings 2019;9(1). https://doi.org/10.3390/buildings9010026.

[11] Chieffo N, Formisano A, Miguel Ferreira T. Damage scenario-based approach and retrofitting strategies for seismic risk mitigation: an application to the historical Centre of Sant'Antimo (Italy). Eur J Environ Civ Eng 2021;25(11):1929–48. https://doi.org/10.1080/19648189.2019.1596164.

[12] Cornell A, Jalayer F, Hamburger RO, Foutch DA. Probabilistic basis for 2000 SAC Federal Emergency Management Agency steel moment frame guidelines. J Struct Eng ASCE 2002;128(4):526–33. https://doi.org/10.1061/ASCE0733-94452002128:4526.

[13] Cornell, C.A., & Krawinkler, H. (2000). *Progress and challenges in seismic performance assessment*. ⟨https://apps.peer.berkeley.edu/news/2000spring/performance.html⟩.

[14] D'Amato M, Laguardia R, Di Trocchio G, Coltellacci M, Gigliotti R. Seismic risk assessment for masonry buildings typologies from L'Aquila 2009 Earthquake Damage Data. J Earthq Eng 2022;26(9):4545–79. https://doi.org/10.1080/13632469.2020.1835750.

[15] Del Gaudio C, De Martino G, Di Ludovico M, Manfredi G, Prota A, Ricci P, Verderame GM. Empirical fragility curves for masonry buildings after the 2009 L'Aquila, Italy, earthquake. Bull Earthq Eng 2019;17(11):6301–30. https://doi.org/10.1007/s10518-019-00683-4.

[16] Del Gaudio C, Di Ludovico M, Polese M, Manfredi G, Prota A, Ricci P, Verderame GM. Seismic fragility for Italian RC buildings based on damage data of the last 50 years. Bull Earthq Eng 2020;18(5):2023–59. https://doi.org/10.1007/s10518-019-00762-6.

[17] Di Pasquale, G., & Goretti, A. (2001). Functional and economic vulnerability of residential buildings affected by recent Italian earthquakes. *In: Proceedings of X Convegno Nazionale "L'Ingegneria Sismica in Italia", 9–13 September 2001 Potenza-Matera, Italy"* . (In Italian).

[18] Dolce M, Goretti A. Building damage assessment after the 2009 Abruzzi earthquake. Bull Earthq Eng 2015;13(8):2241–64. https://doi.org/10.1007/s10518-015-9723-4.

[19] Dolce, M., & Manfredi, G. (2015). Libro bianco sulla ricostruzione privata fuori dai centri storici nei comuni colpiti dal sisma dell'Abruzzo del 6 Aprile 2009. *Rome (IT)*. (In Italian).

[20] Dolce M, Speranza E, Giordano F, Borzi B, Bocchi F, Conte C, Meo A, Di, Faravelli M, Pascale V. Observed damage database of past italian earthquakes: the da.D.O. WebGIS. Boll Di Geofis Teor Ed Appl 2019;60(2):141–64. https://doi.org/10.4430/bgta0254.

[21] D.P.C. Dipartimento della Protezione Civile (2015). Da.D.O. (Database di Danno Osservato) - Piattaforma web-gis per la consultazione e la elaborazione statistica di dati relativi al danno osservato su edifici ordinari danneggiati da eventi sismici di rilevanza internazionale - Manuale di Navigazione Utente. In *Manuale realizzato da EUCENTRE nell'ambito della Convenzione DPC-RELUIS 2015 - Progetto Operativo S3.10* . Allegato S3.10_A. Pavia, Italy. (In Italian).

[22] FEMA. Quantification of Building Seismic Performance Factors. *Report No. FEMA P695. Washington, DC*: Federal Emergency Management Agency; 2009.

[23] Formisano A, Ademovic N. An overview on seismic analysis of masonry building aggregates. Front Built Environ 2022;8. https://doi.org/10.3389/fbuil.2022.966281.

[24] Formisano A, Chieffo N, Clementi F, Mosoarca M. Influence of local site effects on the typological fragility curves for class-oriented masonry buildings in aggregate condition. Open Civ Eng J 2021;15(1):149–64. https://doi.org/10.2174/1874149502115010149.

[25] GNDT/Regione Emilia Romagna/Regione Toscana. Istruzioni per la compilazione della scheda di rilevamento esposizione e vulnerabilità sismica degli edifici. Litogr Della Giunta Reg 1986.

[26] GNTD. (1993). Rischio Sismico di Edifici Pubblici, Parte I: Aspetti Metodologici. *Tipografia Moderna, Bologna, Italy*. (In Italian).

[27] Goretti A, Di Pasquale G. Technical emergency managing. In: Oliveira CS, Roca A, Goula X, editors. Assessing and Managing Earthquake Risk. *The Netherlands*: Kluwer; 2005. p. 339–68.

[28] Grünthal, Gottfried, & European Seismological Commission. Working Group "Macroseismic Scales." (1998). *European macroseismic scale 1998: EMS-98* (Vol. 15). European Seismological Commission, Subcommission on Engineering Seismology, Working Group Macroseismic scales.

[29] Hanks TC, Kanamori H. A moment magnitude scale. J Geophys Res B Solid Earth 1979;84(B5):2348–50. https://doi.org/10.1029/JB084iB05p02348.

[30] Indirli M, Kouris LAS, Formisano A, Borg RP, Mazzolani FM. Seismic damage assessment of unreinforced masonry structures after the Abruzzo 2009 earthquake: The case study of the historical centers of L'Aquila and Castelvecchio Subequo. Int J Archit Herit 2013;7(5):536–78. https://doi.org/10.1080/15583058.2011.654050.

[31] INGV. ShakeMap v4. National Institute of Geophysics and Volcanology; 2016. ⟨http://shakemap.ingv.it/shake4/⟩.

[32] Ioannou I, Bertelli S, Verrucci E, Arcidiacono V, Rossetto T. Empirical fragility assessment of residential buildings using data from the Emilia 2012 sequence of earthquakes. Bull Earthq Eng 2021;19(4):1765–95. https://doi.org/10.1007/s10518-021-01047-7.

[33] ISTAT. 15° Censimento generale della popolazione e delle abitazioni (Italian National Statistics Institute) Popul Hosing Census 2011. ⟨http://dati-censimentopopolazione.istat.it/Index.aspx⟩.

[34] Jalayer F, Cornell CA. Alternative non-linear demand estimation methods for probability-based seismic assessments. Earthq Eng Struct Dyn 2009;38(8):951–72. https://doi.org/10.1002/eqe.876.

[35] Jalayer F, Ebrahimian H, Miano A, Manfredi G, Sezen H. Analytical fragility assessment using unscaled ground motion records. Earthq Eng Struct Dyn 2017;46(15):2639–63. https://doi.org/10.1002/eqe.2922.

[36] Kappos AJ. An overview of the development of the hybrid method for seismic vulnerability assessment of buildings. Struct Infrastruct Eng 2016;12(12):1573–84. https://doi.org/10.1080/15732479.2016.1151448.

[37] Karababa FS, Pomonis A. Damage data analysis and vulnerability estimation following the August 14, 2003 Lefkada Island, Greece, Earthquake. Bull Earthq Eng 2011;9(4):1015–46. https://doi.org/10.1007/s10518-010-9231-5.

[38] Lagomarsino S, Cattari S, Ottonelli D. Derivazione di curve di fragilità empiriche per classi tipologiche rappresentative del costruito Aquilano sulla base dei dati del danno dell'evento sismico del 2009. Res Proj DPC-ReLUIS 2015:*2015*.

[39] Laguardia R, D'Amato M, Coltellacci M, Di Trocchio G, Gigliotti R. Fragility curves and economic loss assessment of RC buildings after L'Aquila 2009 earthquake. J Earthq Eng 2023;27(5):1126–50. https://doi.org/10.1080/13632469.2022.2038726.

[40] Lallemant D, Kiremidjian A, Burton H. Statistical procedures for developing earthquake damage fragility curves. Earthq Eng Struct Dyn 2015;44(9):1373–89. https://doi.org/10.1002/eqe.2522.

[41] Lilliefors HW. On the Kolmogorov-Smirnov test for normality with mean and variance unknown. J Am Stat Assoc 1967;62(318):399–402. https://doi.org/10.1080/01621459.1967.10482916.

[42] Mahoney, M., & Hanson, R.D. (2018a). Seismic performance assessment of buildings, volume 1 - methodology second edition prepared for FEDERAL EMERGENCY MANAGEMENT AGENCY/FEMA *P-58*. ⟨www.ATCouncil.org⟩.

[43] Mahoney, M., & Hanson, R.D. (2018b). Seismic performance assessment of buildings, volume 2 - implementation guide prepared for FEDERAL EMERGENCY MANAGEMENT AGENCY/FEMA P-58. ⟨www.ATCouncil.org⟩.

[44] Medvedev SV. Seismic Intensity Scale MSK-76. *Varsaw*: Publication Institute of Geophysics of Poland, Academy of Sciences; 1977.

[45] Michelini A, Faenza L, Lauciani V, Malagnini L. ShakeMap implementation in Italy. Seismol Res Lett 2008;79(5):688–97. https://doi.org/10.1785/gssrl.79.5.688.

[46] Porter, K. (2021). *A beginner's guide to earthquake fragility vulnerability and risk*. ⟨https://www.sparisk.com/pubs/Porter-beginnersguide.pdf⟩.

[47] Romano F, Faggella M, Gigliotti R, Zucconi M, Ferracuti B. Comparative seismic loss analysis of an existing non-ductile RC building based on element fragility functions proposals. Eng Struct 2018;177:707–23. https://doi.org/10.1016/j.engstruct.2018.08.005.

[48] Rossetto T, D'Ayala D, Ioannou I, Meslem A. Evaluation of existing fragility curves. SYNER-G: typology definition and fragility functions for physical elements at

seismic risk. Dordrecht: Springer; 2014. p. 47–93. https://doi.org/10.1007/978-94-007-7872-6_3.
[49] Rossetto T, Elnashai A. Derivation of vulnerability functions for European-type RC structures based on observational data. Eng Struct 2003;25(10):1241–63. https://doi.org/10.1016/S0141-0296(03)00060-9.
[50] Rossetto T, Ioannou I, Grant DN. Existing empirical fragility and vulnerability functions: compendium and guide for selection. *Pavia*: GEM Technical Report 2015-1 GEM Foundation; 2015.
[51] Rossetto, T., Peiris, N.,Alarcon, J., So, E., Sword-Daniels, V., Libberton, C., Verrucci, E., Del Re, D., Free, M. (2010). The L'Aquila, Italy earthquake of 6 April 2009 apreliminary field report by EEFIT. https://www.istructe.org/resources/report/eefit-mission-report-l-aquila-italy/.
[52] Rossi L, Stupazzini M, Parisi D, Holtschoppen B, Ruggieri G, Butenweg C. Empirical fragility functions and loss curves for Italian business facilities based on the 2012 Emilia-Romagna earthquake official database. Bull Earthq Eng 2020;18(4):1693–721. https://doi.org/10.1007/s10518-019-00759-1.
[53] Rosti A, Rota M, Penna A. Empirical fragility curves for Italian URM buildings. Bull Earthq Eng 2021;19(8):3057–76. https://doi.org/10.1007/s10518-020-00845-9.
[54] Rota M, Penna A, Strobbia CL. Processing Italian damage data to derive typological fragility curves. Soil Dyn Earthq Eng 2008;28(10–11):933–47. https://doi.org/10.1016/j.soildyn.2007.10.010.
[55] Sabetta F, Goretti A, Lucantoni A. Empirical fragility curves from damage Surveys and estimated strong ground motion. Proc 11th Eur Conf Earthq Eng 1998:1–11.
[56] Shinozuka M, Feng MQ, Lee J, Naganuma T. Statistical analysis of fragility curves. J Eng Mech 2000;126(12):1224–31. https://doi.org/10.1061/(ASCE)0733-9399(2000)126:12(1224).
[57] Sieberg A. Geologie der Erdbeben. Handb Der Geophys 1930;2(4):552–5 (In German).
[58] Spence RJS, Coburn AW, Pomonis A, Sakai S. Correlation of ground motion with building damage: the definition of a new damage-based seismic intensity scale. Proceedings of the 10th World Conference of Earthquake Engineering. *Rotterdam*: AA Balkema; 1992. p. 551–6.
[59] Tatangelo M, Audisio L, D'Amato M, Gigliotti R. Seismic risk analysis on masonry buildings damaged by L'Aquila 2009 and Emilia 2012 earthquakes. Procedia Struct Integr 2022;44:990–7. https://doi.org/10.1016/j.prostr.2023.01.128.
[60] Tatangelo, M., Audisio, L., D'Amato, M., & Gigliotti, R. (2023). Typological seismic losses assessment by damaged masonry buildings after L'Aquila 2009 and Emilia 2012 earthquakes. *COMPDYN 2023, Proceedings of the 9th ECCOMAS Thematic Conference on Computational Methods in Structural Dynamics and Earthquake Engineering*, *1*, 1071–1083. ⟨https://2023.compdyn.org/proceedings/pdf/20639.pdf⟩.
[61] Vamvatsikos D, Cornell AC. Incremental dynamic analysis. Earthq Eng Struct Dyn 2002;31(3):491–514. https://doi.org/10.1002/eqe.141.
[62] Vamvatsikos D, Cornell CA. Direct estimation of the seismic demand and capacity of oscillators with multi-linear static pushovers through IDA. Earthq Eng Struct Dyn 2006;35(9):1097–117. https://doi.org/10.1002/eqe.573.
[63] Whitman, R.V., Reed, J.W., & Hong, S.-T. (1973). Earthquake damage probability matrices. In: Proceedings of the 5th World Conference on Earthquake Engineering.
[64] Wood HO, Neumann F. Modified Mercalli Intensity scale of 1931. Bull Seismol Soc Am 1931;21(4):277–83. https://doi.org/10.1785/BSSA0210040277.
[65] Zuccaro G, Cacace F. Seismic vulnerability assessment based on typological characteristics. The first level procedure "SAVE". Soil Dyn Earthq Eng 2015;69:262–9. https://doi.org/10.1016/j.soildyn.2014.11.003.
[66] Zuccaro G, Perelli FL, De Gregorio D, Cacace F. Empirical vulnerability curves for Italian mansory buildings: evolution of vulnerability model from the DPM to curves as a function of accelertion. Bull Earthq Eng 2021;19(8):3077–97. https://doi.org/10.1007/s10518-020-00954-5.
[67] Zucconi M, Ferlito R, Sorrentino L. Simplified survey form of unreinforced masonry buildings calibrated on data from the 2009 L'Aquila earthquake. Bull Earthq Eng 2018;16(7):2877–911. https://doi.org/10.1007/s10518-017-0283-7.
[68] Zucconi M, Romano F, Ferracuti B. Typological fragility curves for RC buildings: influence of damage index and building sample selection. Eng Struct 2022;266. https://doi.org/10.1016/j.engstruct.2022.114627.
[69] Zucconi M, Sorrentino L, Ferlito R. Principal component analysis for a seismic usability model of unreinforced masonry buildings. Soil Dyn Earthq Eng 2017;96:64–75. https://doi.org/10.1016/j.soildyn.2017.02.014.